# COLLISION-INDUCED SPECTRA OF DOUBLE VIBRATIONAL TRANSITIONS OF $H_2$ ($V=1 \leftarrow 0$) + $N_2$ ($V=1 \leftarrow 0$) AT 201 K AND 298 K



CLIFF STAMP

# INFORMATION TO USERS

This manuscript has been reproduced from the microfilm master. UMI films the text directly from the original or copy submitted. Thus, some thesis and dissertation copies are in typewriter face, while others may be from any type of computer printer.

**The quality of this reproduction is dependent upon the quality of the copy submitted.** Broken or indistinct print, colored or poor quality illustrations and photographs, print bleedthrough, substandard margins, and improper alignment can adversely affect reproduction.

In the unlikely event that the author did not send UMI a complete manuscript and there are missing pages, these will be noted. Also, if unauthorized copyright material had to be removed, a note will indicate the deletion.

Oversize materials (e.g., maps, drawings, charts) are reproduced by sectioning the original, beginning at the upper left-hand corner and continuing from left to right in equal sections with small overlaps.

Photographs included in the original manuscript have been reproduced xerographically in this copy. Higher quality 6" x 9" black and white photographic prints are available for any photographs or illustrations appearing in this copy for an additional charge. Contact UMI directly to order.

Bell & Howell Information and Learning
300 North Zeeb Road, Ann Arbor, MI 48106-1346 USA
800-521-0600

# COLLISION-INDUCED SPECTRA OF DOUBLE VIBRATIONAL TRANSITIONS OF $H_2$ ($V = 1 \leftarrow 0$) + $N_2$ ($V = 1 \leftarrow 0$) AT 201 K AND 298 K

By

©Cliff Stamp

A THESIS SUBMITTED IN PARTIAL

FULFILLMENT OF THE REQUIREMENTS

FOR THE DEGREE OF

MASTERS OF SCIENCE

DEPARTMENT OF PHYSICS AND PHYSICS OCEANOGRAPHY

MEMORIAL UNIVERSITY OF NEWFOUNDLAND

JUNE, 1999

ST. JOHN'S NEWFOUNDLAND

## Acknowledgements

I express my appreciation to my supervisor, Professor S. P. Reddy for his guidance and encouragement throughout the progress of this research project and in the preparation of this thesis.

I would like to thank Dr. Paul Gillard for his help in the experimental work, numerical analysis, computer programming, and theoretical considerations, without whose help many problems would never have been solved. In addition, I would like to thank Dr. J. C. Lewis for very helpful discussions pertaining to various theoretical considerations and numerical analysis. Also, I would like to mention Drs. Robert Le Roy, Chris Benner, and James K. G. Watson, for helpful discussions on general matters concerning numerical analysis, in particular least squares fitting procedures and interpretation of results.

I also acknowledge the financial support received from Professor Reddy's NSERC grant. I am also grateful to Memorial University of Newfoundland for an F. A. Aldrich Graduate Award and to MUN Graduate School for the support in the form of a Graduate Fellowship.

## Abstract

In the present research project a systematic experimental study of the collision-induced absorption (CIA) spectra of the double fundamental vibrational transitions $H_2(v = 1 \leftarrow 0) + N_2(v = 1 \leftarrow 0)$ was undertaken for the first time in the spectral region 5600 - 7600 $cm^{-1}$ . The experiments were carried out with a 2.0 m high-pressure, low-temperature transmission cell in binary mixtures of $H_2$ and $N_2$ at 201 K and 298 K for partial densities of $H_2$ and $N_2$ in the ranges 60 to 400 and 100 to 350 amagat, respectively.

The observed spectra are interpreted in terms of the double transitions : $O_1(3) + Q_1(J)$ , $O_1(2) + Q_1(J)$ , $Q_1(J) + O_1(J)$ , $Q_1(J) + Q_1(J)$ , $Q_1(J) + S_1(J)$ , $S_1(0) + Q_1(J)$ , $S_1(1) + Q_1(J)$ , $S_1(2) + Q_1(J)$ , and $S_1(3) + Q_1(J)$ , in which the first component is from $H_2$ and the second component is from $N_2$. These transitions occur on the high wavenumber wing of the enhancement of the CIA fundamental band of $H_2$ in $H_2$-$N_2$ mixtures. Various semi-empirical line shapes were attempted in the analysis of the observed spectra. Lewis-Birnbaum-Cohen (LBC) lineshape function is found to give the best fit of the calculated profiles to the experimental profiles. The lineshape parameters $\tau_1$, and $\tau_2$ are found to have a linear dependence on the partial density of $\rho_{N_2}$ of nitrogen. In particular, $\tau_1$ increases with $\rho_{N_2}$, thus showing pressure-narrowing of the linewidth parameter $\delta_1$ $(= 1/2\pi c\tau_1)$ as the density increases. Finally the binary and ternary absorption coefficients of the double vibrational transitions of $H_2$+$N_2$ were calculated.

## Contents

## List of Tables

## List of Figures

# Chapter 1

# Introduction

## 1.1 Collision-Induced Absorption

Isolated homonuclear diatomic molecules such as $H_2$, $D_2$, $N_2$, and $O_2$, in their ground electronic states do not possess permanent static or oscillatory electric dipole moments because of the symmetry of their charge distribution. Consequently, these molecules, unlike their polar counter species, have no electric dipole absorption (i.e. allowed transitions) at their vibrational and rotational frequencies. However they do have higher order multipole moments such as quadrupole moment, hexadecapole moment, tetrahexadecapole moment, etc. Collision-induced absorption (CIA) occurs in these molecules in the pure gases or in mixtures with other gases as a result of transient electric dipole moments induced in them during binary or higher order collisions. The induction mechanisms include short-range electron overlap induction resulting from the distortion of electron clouds, and various multipolar inductions resulting from the polarization of one molecule by the corresponding multipolar field of its collision partner. In CIA spectra, normally forbidden transitions occur.

Collision-Induced Absorption was discovered in 1949 in compressed $N_2$ and $O_2$ in the regions of their fundamental bands by Crawford et al.[1]. Later in the same year CIA of the fundamental band of $H_2$ was also reported by Welsh et. al.[2]. In the past fifty years, CIA spectra of the fundamental and overtone bands of $H_2$ in the pure gas and in binary mixtures with other simple gases have been studied in considerable detail over a wide

range of experimental conditions. Some studies of the CIA spectra of $N_2$ in the pure gas in some binary mixtures with other gases have also been made.

## 1.2 Background Information on CIA Spectra of $H_2$ and $N_2$

There has been a great interest in the study of the spectra of $H_2$ because of several reasons which include the following: $H_2$ is the simplest of all stable diatomic molecules; theoretical calculations can be carried out for it more rigorously; and in spite of the broad nature of the collision-induced spectra of $H_2$, the rotational components of its bands are somewhat separate because of its small moments of inertia (i.e., its large rotational constant). Molecular hydrogen is the constituent of the outer planets of the solar system, cool stars and interstellar space. As a matter of fact, molecular hydrogen is the most abundant species in the universe. The earth's atmosphere mainly consists of $N_2$ and $O_2$ plus small quantities of other gases such as CO and $CO_2$, etc. . Like $H_2$, $N_2$ and $O_2$ do not have allowed infrared spectra because of the lack of permanent electric dipole moments; however they do have CIA spectra in the infrared region. Thus CIA spectra are important in understanding the processes involved in the planetary and some stellar spectra and the earth's atmospheric spectra.

In 1972 Welsh[3] provided a comprehensive review of the experimental work done on CIA spectra of gaseous $H_2$ prior to 1971. In 1985 Reddy[4] gave an exhaustive review of the more recent work on the collision-induced vibrational absorption of $H_2$, $D_2$, and HD in the gaseous phase. For further information on CIA, the reader is referred to Reddy et. al.[4] and Hsieh[5]. Reddy et. al.[4] reported simultaneous vibrational transitions corresponding to the triple collisions of the type $H_2 - H_2 - H_2$ in the region of the second overtone band of $H_2$. Comprehensive bibliographies on this subject have been prepared by Rich and McKellar (1976)[6], and Hunt and Poll (1986)[7]. Van Kranendonk (1974)[8],

Poll (1980)[9], and Birnbaum et. al. (1982)[10] have reviewed the theoretical aspects of CIA. In a textbook on the phenomenon of CIA in gaseous phase Frommhold (1993)[11] summarised many aspects of the theory and gave exhaustive references on the subject.

The induced-dipole moment in colliding pairs of molecules is usually represented by the so-called "exponential-4" model by Van Kranendonk[12] and Poll and Van Kranendonk[13]. Poll and Hunt [14] gave angle-dependent expressions for the induced-dipole moment. In the "exponential-4" model, the induced dipole moment $\mu$ in a pair of colliding molecules consists of two additive parts, $\mu_{overlap}(R)$ arising from the overlap of the electron clouds of the colliding molecules , and $\mu_{quad}(R)$ resulting from the polarisation of one molecule by the quadrupole field of the other. R being the intermolecular separation. The quantity $\mu_{overlap}$ decreases as a function of $e^{-R}$ and $\mu_{quad}$ varies asymptotically as $R^{-4}$. Pair potentials $\Phi(r_i, r_j, R_{ij})$ represent binary collisions, and potentials involving terms such as $\Phi(r_i, r_j, r_k, R_{ij}, R_{jk}, R_{kl})$ take into account higher order collisions.

The overlap induced-dipole moment $\mu_{overlap}$ is mostly isotropic and gives rise to the broader $Q_{ov}(J)(\Delta J = 0)$ transitions, J being the rotational quantum number. The anisotropic part of the induced-dipole moment contributes to the intensity of the $O(\Delta J = -2)$ , $Q(\Delta J = 0)$, and $S(\Delta J = +2)$ transitions. One of the distinct features of the overlap induction is the occurrence of a characteristic "dip" in the band at the position of the corresponding free molecular transition. An insight into this "dip" was given by Van Kranendonk[15] in terms of a destructive interference between the induced dipoles in successive collisions. A detailed kinetic theory of this phenomenon was given by Lewis and Van Kranendonk[16, 17, 18] and Lewis[19, 20, 21, 22, 23]. The quadrupole-induced dipole moment $\mu_{quad}$ is dependent on the matrix elements of the quadrupole moment and the polarizability of the colliding molecules. The isotropic component of the polarizability of a colliding molecule contributes to the absorption intensity of the transitions $O(\Delta J =$

$-2)$, $Q(\Delta J = 0)$, and $S(\Delta J = +2)$. It gives rise to several double transitions of the type $O_{\Delta v}(J_1) + Q_0(J_2), Q_{\Delta v}(J_1) + Q_0(J_2), S_{\Delta v}(J_1) + Q_0(J_2), Q_{\Delta v}(J_1) + Q_{\Delta v}(J_2), Q_{\Delta v}(J_1) + S_{\Delta v}(J_2), S_{\Delta v}(J_1) + Q_{\Delta v}(J_2)$. The subscripts $\Delta v (= v' - v")$ represent the change in the vibrational quantum number and take values 0,1,2,..., etc., and subscripts 1 and 2 of $J$ refer to molecules 1 and 2 in a binary collision. The anisotropic component of the polarizability, on the other hand, contributes a small amount to the transitions given above and to the double transitions $S_{\Delta v}(J_1) + S_{\Delta v}(J_2)$. In a "single" transition, only one molecule of the colliding pair makes a vibration or a vibration-rotation transition while the other molecule makes an orientational transition denoted by $Q_0(J)$ with no change in internal energy. In a "double" transition, both molecules of the colliding pair simultaneously absorb a single photon and change their internal energies.

In addition to the components $\mu_{overlap}(R)$ and $\mu_{quad}(R)$, the induced-dipole moment consists of weaker components such as $\mu_{hexa}(R)$, $\mu_{tetra-hexa}(R)$ , etc. . Of these, $\mu_{hexa}(R)$ results from the polarisation of one molecule by the hexadecapole field of its collision partner and gives rise to weaker transitions corresponding to $\Delta$J=0, $\pm$2, and $\pm$4. The transitions corresponding to $\Delta$J=+4 are known as U transitions. In the CIA spectra of the fundamental band of $H_2$, U transitions , first observed by Gibbs et. al., (1974), have been studied in detail and analysed by Reddy et. al. (1980). The $\mu_{tetra-hexa}(R)$ component comes from the polarisation of a molecule by the tetra-hexadecapole field of its collision partner. This gives rise to very weak transitions corresponding to $\Delta$J=0, $\pm$ 2, $\pm$ 4 and $\pm$ 6. Okumura et al. (1989) reported the pure rotational transition $W_0(J)$ corresponding to $\Delta J = +6$ in solid $H_2$.

McKellar and Welsh[24] studied the first overtone region of $H_2$ in the pure gas and in binary mixtures with Ar and $N_2$ with a path length of 137 m in the temperature range 85 to 116 K and analysed the absorption profiles. The analysis revealed that systematic discrepancies exist between the experimental and calculated profiles. The

isotropic overlap induction mechanism is found to contribute greatly to the intensity of the fundamental band of $H_2$[25] but it does not contribute to the intensity of its first overtone band[24, 26, 27, 28]. De Remgis[29] observed a decrease in the half-width of the quadrupole-induced transition (known as pressure-narrowing) in the fundamental band of $H_2$ in $H_2$-Ar mixtures for gas densities above 300 amagat. Subsequently, Mactaggart et. al. [30] studied this effect in the fundemental band of $H_2$ in $H_2$-Ar, $H_2$-Kr, and $H_2$-Xe.

The CIA of the fundamental band of $N_2$ observed in the pure gas by Crawford et. al.[1] was investigated by Reddy and Cho[31] in pure $N_2$ and in its binary mixtures with $H_2$, Ar, and $H_2$ at room temperature and by Shapiro and Gush[32] in pure $N_2$ and $N_2$-Ar mixtures also at room temperature. The reader is referred to Laffery et. al.[33] and Frommhold[11] for detailed references on the CIA spectra of the fundamental band of $N_2$.

## 1.3 Double vibrational transitions in CIA Spectra

At room temperature almost all the molecules in normal $H_2$ are distributed among the rotational levels J=0 to 3 of the lowest vibrational state v=0 of its ground electronic state $^1\Sigma_g{}^+$. In the CIA spectrum of the fundamental band of $H_2$ in the pure gas, based on the consideration of the overlap and quadruploar induction mechanisms, the following transitions occur : $O_1(J)+Q_0(J), Q_1(J)+Q_0(J), S_1(J)+Q_0(J), Q_1(J)+S_0(J), S_1(J)+S_0(J)$. In the standard spectroscopic notation, the O, Q, and S branches correspond to the rotational selection rule $\Delta J$ = -2,0, and +2, respectively; subscripts 1 and 0 represent the change in the vibrational quantum number, $\Delta v(= v' - v'')$, and $Q_0(J)$ represents an orientational transition with no corresponding change in frequency. The so-called 'single' transitions $O_1(J)$, $Q_1(J)$, and $S_1(J)$ are really $O_1(J) + Q_0(J)$, $Q_1(J) + Q_0(J)$ and $S_1(J)+Q_0(J)$, respectively. The possible 'single' transitions in the CIA fundamental band of $H_2$ at room temperature are shown in an energy level diagram in Figure 1.1 in

which the energy levels are calculated from the constants of the free $H_2$ molecule[34].

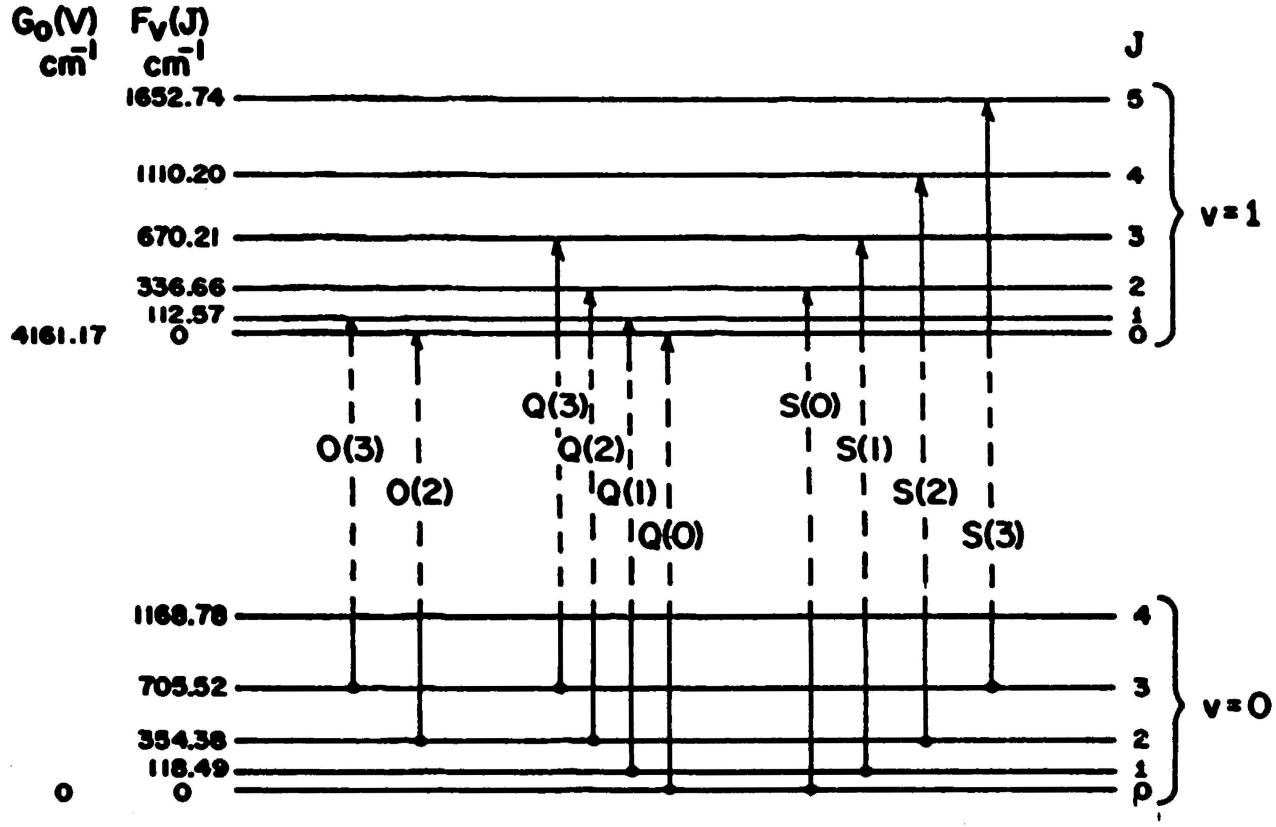


Figure 1.1: 'Single' transitions in the CIA fundamental band of $H_2$ at room temperature

Collision-induced absorption spectra of the double vibrational transitions $H_2(v = 1, J' \leftarrow v = 0, J) + N_2(v = 1, J' \leftarrow v = 0, J)$ occur in the region 5600 - 7600 $cm^{-1}$. The wavenumbers of the vibrational and rotational levels of $H_2$ and $N_2$ are separately calculated from the molecular constants of free $H_2$ and free $N_2$[35, 36] molecules. These constants are listed in Table 1.1 . The $O_1(J)$, $Q_1(J)$, and $S_1(J)$, transitions in the fundamental bands of $H_2$ and $N_2$ were calculated by using the following equation

$$\nu_{O,Q,S} = \nu_{10} + F'_v(J') - F''_v(J'') \ . \tag{1.1}$$

where

$$F_v(J) = B_v J(J+1) - D_v J^2(J+1)^2 + H_v J^3(J+1)^3 + \ldots \tag{1.2}$$

Here $\nu_{10}(= Q_1(0))$ is the fundamental band-center wavenumber, and $B_v$, $D_v$, and $H_v$ are the usual rotational parameters.

## 1.4 Present work

It is the aim of the present research project to make a systematic investigation of the CIA spectra of the double vibrational transitions $H_2(v = 1, J' \leftarrow v = 0, J) + N_2(v = 1, J' \leftarrow v = 0, J)$. Prior to the present work there was one brief mention of an absorption peak at 6500 $cm^{-1}$ in the double vibrational spectrum of $H_2$+$N_2$ by Vodar[37] in 1959.

The experiments were carried out with a 2.0 m high-pressure low-temperature transmission-type absorption cell at 201 and 298 K in binary mixtures of $H_2$ and $N_2$ with partial densities of $H_2$ and $N_2$ in the range of 60 to 400 and 100 to 350 amagat, respectively. A Perkin-Elmer model 112 double pass spectrometer equipped with an LiF prism, an uncooled PbS detector and a microprocessor-controlled stepping motor was used to record

Table 1.1: Molecular constants used in the calculation of the energy levels.

| Vibrational level v | Constant ($cm^{-1}$) | |
|---|---|---|
| | $\underline{H_2}$ | |
| 0 | $B_0$ : | 59.334511 |
| | $D_0$ : | 0.0456517 |
| | $H_0$ : | 4.562 X $10^{-5}$ |
| 1 | $\nu_{10}$ : | 4161.1687 |
| | $B_1$ : | 56.37421 |
| | $D_1$ : | 0.044051 |
| | $H_1$ : | 4.323 X $10^{-5}$ |
| | $\underline{N_2}$ | |
| 0 | $B_0$ : | 1.989574 |
| | $D_0$ : | 5.76 X $10^{-6}$ |
| 1 | $\nu_{10}$ : | 2329.9168 |
| | $B_1$ : | 1.972182 |
| | $D_1$ : | 5.752 X $10^{-6}$ |

the spectra.. Background water vapour absorption was reduced to a stable level by flushing the path of the radiation with dry nitrogen gas continuously. The apparatus and experimental details are described in Chapter 2.

Theoretical aspects including the lineshape functions used in the profile analysis of the observed spectra are presented in Chapter 3.

The observed spectra are interpreted in terms of the double transitions : $O_1(3) + Q_1(J)$ , $O_1(2) + Q_1(J)$ , $Q_1(J) + O_1(J)$ , $Q_1(J) + Q_1(J)$ , $Q_1(J) + S_1(J)$ , $S_1(0) + Q_1(J)$ , $S_1(1) + Q_1(J)$ , $S_1(2) + Q_1(J)$ , and $S_1(3) + Q_1(J)$ , the first component from $H_2$ and the second component from $N_2$. These transitions occur on the high frequency wing of the CIA fundamental band of $H_2$. Various semi-empirical lineshapes were attempted in the analysis of the observed spectra. Lewis-Birnbaum-Cohen[38, 39] lineshape function was found to give satisfactory fits of the calculated profiles to the experimental profiles. Lineshape parameters and absorption coefficients obtained from the analysis are reported. The experimental absorption profiles and the results of the analysis are presented in Chapter 4.

A summary of the present research project is given in Chapter 5.

Appendix A is devoted to methods of analysis and relevant descriptive statistics.

A brief note on the astrophysical applications of CIA spectra is presented in Appendix B.

# Chapter 2

## Apparatus and Experimental Details

Collision-induced absorption spectra of the double vibrational transitions of $H_2(v' = 1, J' \leftarrow v'' = 0, J'') + N_2(v' = 1, J' \leftarrow v'' = 0, J'')$ were recorded at temperatures 201 K and 298 K. The experimental setup consisted mainly of a 2 m high-pressure, low-temperature, stainless-steel absorption cell, a gas handling system, an infrared spectrometer and a microprocessor-controlled data acquisition system. Details of the apparatus and the experimental techniques are presented in this chapter.

### 2.1 The 2 m Absorption Cell

The 2 m long, transmission-type absorption cell,designed and constructed earlier in our laboratory[40] for work with gases at high pressures up to 2000 atmospheres and temperatures in the range 77 to 298 K, was used in the present work at 201 K and 298 K for gas densities up to 400 amagat of $H_2 - N_2$ mixtures. A schematic diagram of a cross section of one end of the cell is shown in Figure 2.1. The absorption cell T was constructed from type 303 stainless-steel tube, 2 m long, with a 7.62 cm outer diameter and 2.54 cm inner diameter (with a wall thickness of 2.54 cm). The polished light guide L was made in five sections and has a rectangular aperture, 1.00 cm high x 0.50 cm wide. A sapphire window $W_1$, 2.54 cm in diameter and 1.00 cm thick, was attached to the polished stainless steel window seat S having a circular aperture of 1.00 cm, with General Electric Silicone Sealant. With invar O-ring $R_1$ between the window seat and the absorption cell, a pressure-tight seal was secured by tightening a stainless steel piece

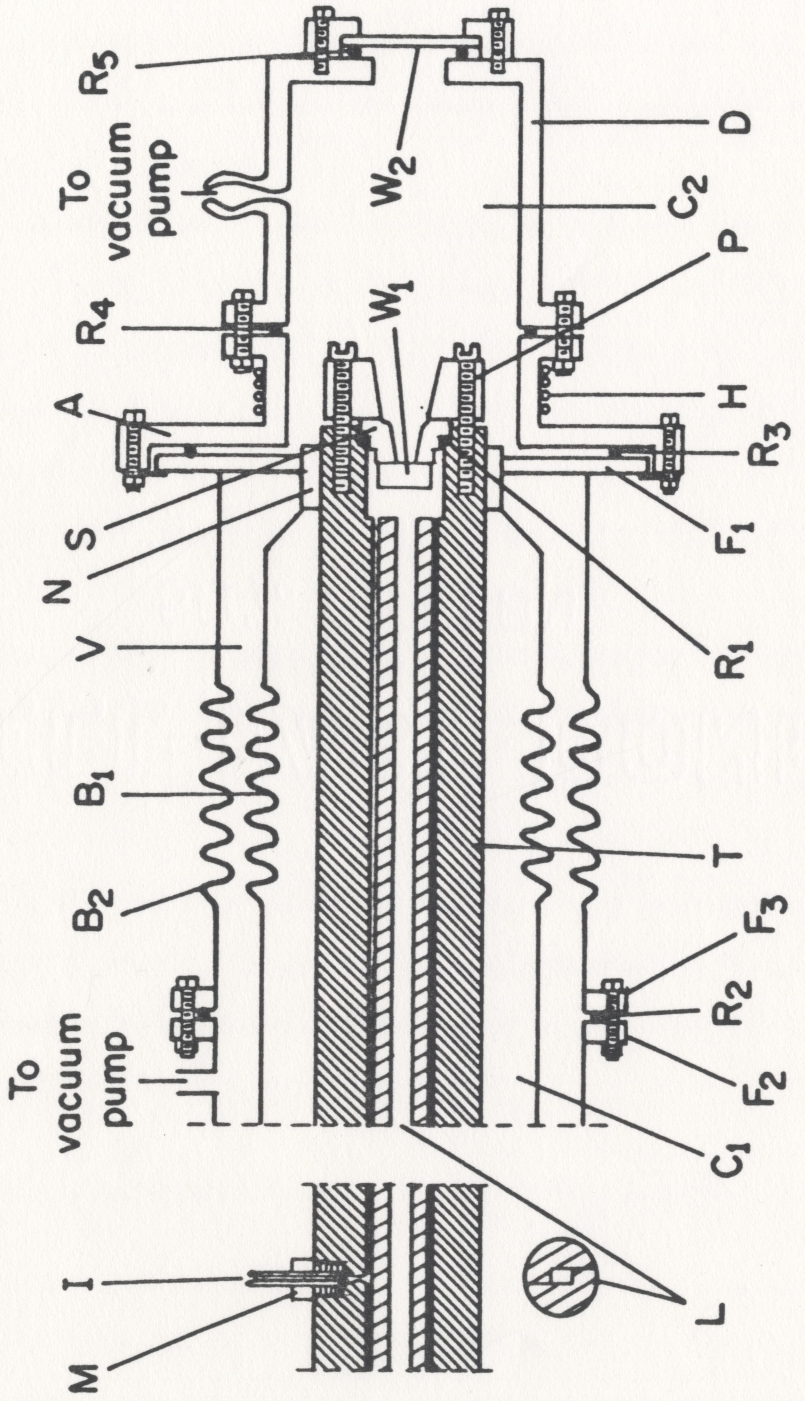


Figure 2.1: A cross sectional view of one end of the 2 m absorption cell (See text for details of the symbols).

P against the cell body by means of eight Allen head bolts. A stainless steel capillary tube with a diameter of 0.64 cm was connected to the cell body by means of an Aminco fitting M to act as the gas inlet I.

A stainless-steel nut N, 1.50 cm long and 7.62 cm in inner diameter, was threaded onto the end of the cell and welded onto it. A flange $F_1$ and bellows $B_1$ (10.16 cm in diameter), both made from stainless steel, were welded to a stainless-steel cone. Bellows $B_2$ (16.5 cm in diameter) and flanges $F_2$ and $F_3$ were also made of stainless steel. These two bellows allow relative expansion and contraction of the absorption cell and the vacuum jacket V. A neoprene O-ring $R_2$, maintained between the tightened flanges $F_2$ and $F_3$ allowed a good vacuum seal. For low temperature experiments, chamber $C_1$ is to be filled with a coolant such as liquid nitrogen or alcohol-dry ice mixture. The end vacuum chamber $C_2$ is 10.0 cm long and 10.5 cm in diameter. A vacuum-tight seal was provided by means of a silicone rubber O-ring $R_3$, maintained between flange $F_1$ and an aluminium cap A, and a neoprene O-ring $R_4$ between the aluminium cap and the Delrin end cap D. A sapphire window $W_2$, 0.30 cm thick and 5.08 cm in diameter, was sealed to D with neoprene O-ring $R_5$ between $W_2$ and D. The purpose of the vacuum chamber $C_2$ is to prevent frosting on the cell window $W_1$ in the low temperature experiments. Freezing is prevented by means of a heating tape wound around the cap A.

## 2.2 The Experimental Setup and the Optical Layout

The experimental setup and the optical arrangement is shown schematically in Figure 2.2(a). The light source L is a General Electric FFJ Quartzline lamp which gives continuous radiation in the near infrared and visible regions. It is housed in a water-cooled brass jacket designed in our laboratory and was operated at a voltage of 90 V, controlled by a General Radio USA Variac (model WJOMT3A transformer) stabilised by a

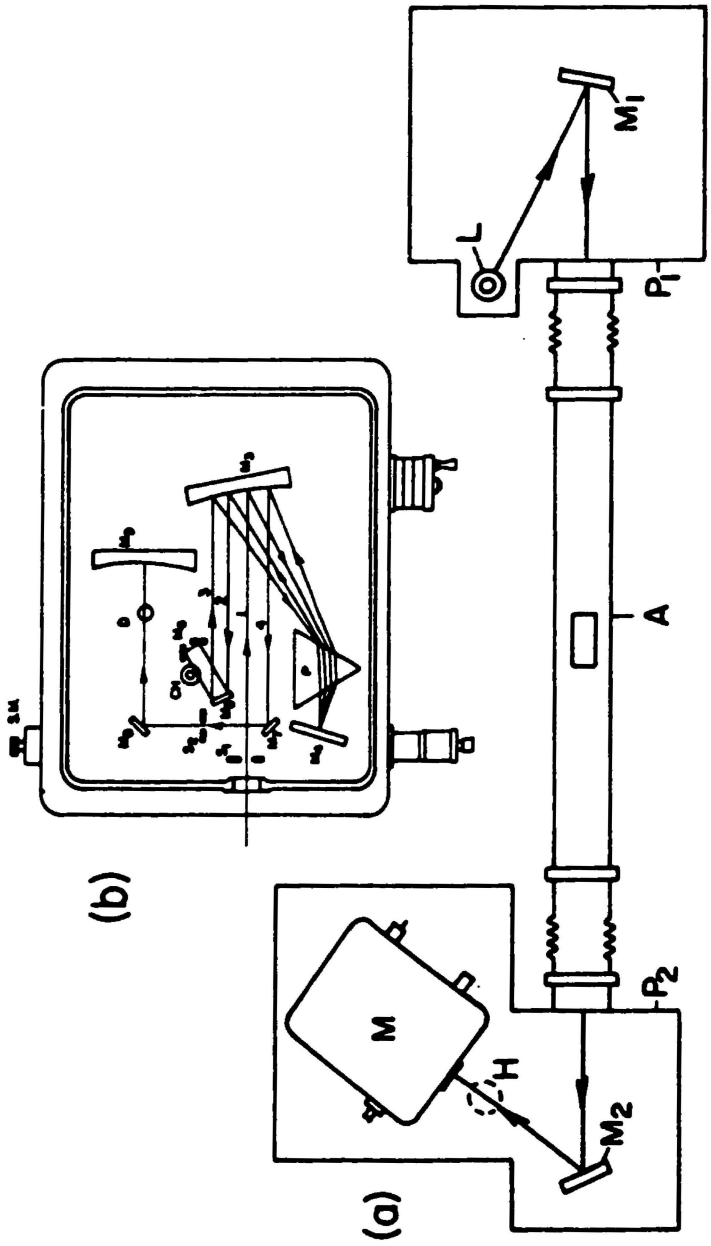


Figure 2.2: Caption is given on the following page.

Figure 2.2 : (a) A schematic diagram of the experimental setup. L : source of radiation; $M_1$ and $M_2$ : spherical mirrors; A: absorption cell; M: Perkin-Elmer model 99 monochromator, $P_1$ and $P_2$ : Plexiglas boxes. (b) Path of the monochromatic radiation inside monochromator. $S_1$ and $S_2$ : entrance and exit slits ; $M_3$ : a $21^o$ off-axis parabolic mirror ; P : prism; $M_4$ : littrow mirror; $M_5 - M_8$ : plane mirrors; $M_9$ : a parabolic mirror; CH : tuning fork chopper; D : PbS detector; SM : stepping motor.

Sorensen ACR 2000 voltage regulator. The radiation from the source was focused on the entrance window of the absorption cell by a front-coated concave mirror $M_1$ . Radiation transmitted by the absorption cell was then focused by another concave mirror $M_2$ onto the entrance slit of a Perkin-Elmer model 99 single-beam double-pass monochromator M, equipped with a lithium fluoride (LiF) prism and an uncooled lead sulphide (PbS) detector D. The optical path of monochromatic radiation inside the monochromator is shown in Figure 2.2(b). The focused radiation after the first pass (beams 1 and 2) in the monochromator was chopped by a 260 Hz tuning-fork chopper CH, model L-40, supplied by American time products, and reflected back to the prism for a second pass (beams 3 and 4). The radiation was then focused onto the exit slit of the monochromator and subsequently onto the PbS detector by a parabolic mirror $M_9$. The linear response of the PbS detector with the intensity of the incident radiation was checked by earlier researchers in our laboratory and was found to be satisfactory. The slit width of the spectrometer maintained at 35 $\mu$m gave a spectral resolution of 13 $cm^{-1}$ at 7500 $cm^{-1}$. A mercury lamp H can be inserted in the optical path for calibration purposes when necessary. Since this lamp blocks the light from the continuous light source, calibration spectra cannot be recorded simultaneously with the actual CIA spectra.

The entire optical path outside the absorption cell was contained within two airtight Plexiglas boxes $P_1$ and $P_2$ (Figure 2.2(a)). Both boxes were flushed continuously during the entire experiment with dry nitrogen gas produced by evaporating liquid nitrogen in a 200 litre dewar with a small electrical heater (a 100 $\Omega$ 25 W resistor). The inlet and outlet of the Plexiglas boxes consist of two one-way plastic valves (not shown in the Figure). It took about 4 to 5 days to reduce atmospheric water vapour absorption to a stable reduced level.

## 2.3 The Data Acquisition System

A block diagram of the signal detection and recording system is shown in Figure 2.3. The signal from the PbS detector is first sent to a lock-in amplifier, model SR510, with a built-in preamplifier, supplied by Standford Research Systems. The signal from the lock-in amplifier was sent to the decade divider, model DV412, supplied by Electro-Measurement Inc., for attenuation. The attenuated signal was then sent to a microprocessor-controlled analog-to-digital converter (ADC) which in turn transmitted the data to a computer for storage and analysis.

The microprocessor-controlled stepping motor system was earlier designed and built in our laboratory[41]. The original hardware has not been modified since that time. However, a few improvements have been made to the data acquisition software. The first alteration to the software was the addition of code to calculate a large sample standard deviation for the recorded intensity measurements. This standard deviation was calculated at the start and at the end of the spectrum. It was usually less than 1.0 % and not significantly different at either end and was used to estimate the required number of traces needed to average in order to obtain a practical minimum standard error. An infinite reduction in noise cannot be achieved, even though the random noise was well modelled by a gaussian distribution, because the distribution is discreet and the intervals (on the order of about 0.1%) set an absolute lower bound for a meaningful standard error. The second modification was the addition of code which allowed sampling of more than one point per drum number (see section 2.6) in order to reduce the spectral noise. Thirdly, the code was further modified to allow the data to be collected continuously at preset time intervals (for example, every half hour). Finally, a few lines of code were added so that the data files were time-stamped and included an appropriate comment such as:

H2-N2 : Exp. 8 : 298 K : Slit at 55 : Drum at 4.00 21-7-98 09:30:15 09:22:15

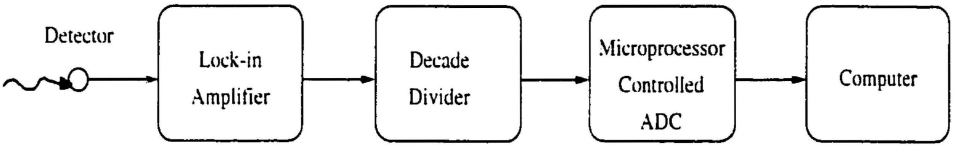


Figure 2.3: A block diagram of the signal detection system.

which describes the specifics of the experiment.

## 2.4 The Gas-Handling System

The gas-handling system used in the present work is shown schematically in Figure 2.4.

Thermal compressors $T_1$ and $T_2$ (pressure limits $\approx$ 7500 psi) and $T_3$ and $T_4$ (pressure limits $\approx$ 25000 psi) were made of stainless steel. The required pressures were obtained by filling a thermal compressor with gas at cylinder pressure, cooling it with liquid nitrogen, then refilling it with gas from another similar thermal compressor, pressurised with cylinder pressure gas, and repeating the procedure as necessary. The low pressure compressors were used to obtain the needed base densities for $H_2$, and the high pressure compressors were used to obtain the required high pressures of $N_2$. Gauges $G_1$, $G_2$, and $G_3$ are Ashcroft Bourdon tube gauges, supplied by Dresser Industries, Inc. The gauges were calibrated against a test gauge, which in turn was calibrated against an Ashcroft dead-weight pressure balance which has an accuracy of 0.1% (these calibrations were performed by earlier researchers in our laboratory). The ranges of $G_1$, $G_2$, and $G_3$ are 0-20,000 (40), 0-5,000 (10), and 0-10,000 (20) psi, respectively. The bracketed numbers are the estimated measurement uncertainties due to judgement error in reading the gauges, and are set to 1/5 of the smallest division on the analog display. All fittings in the gas handling system, expect the copper coil and the gas cylinders, were Aminco stainless steel high-pressure fittings, rated for pressures up to 60,000 psi . Ultra high-purity grade $H_2$ and research grade $N_2$, both supplied by Matheson Gas Products, Canada, were used in the experiments.

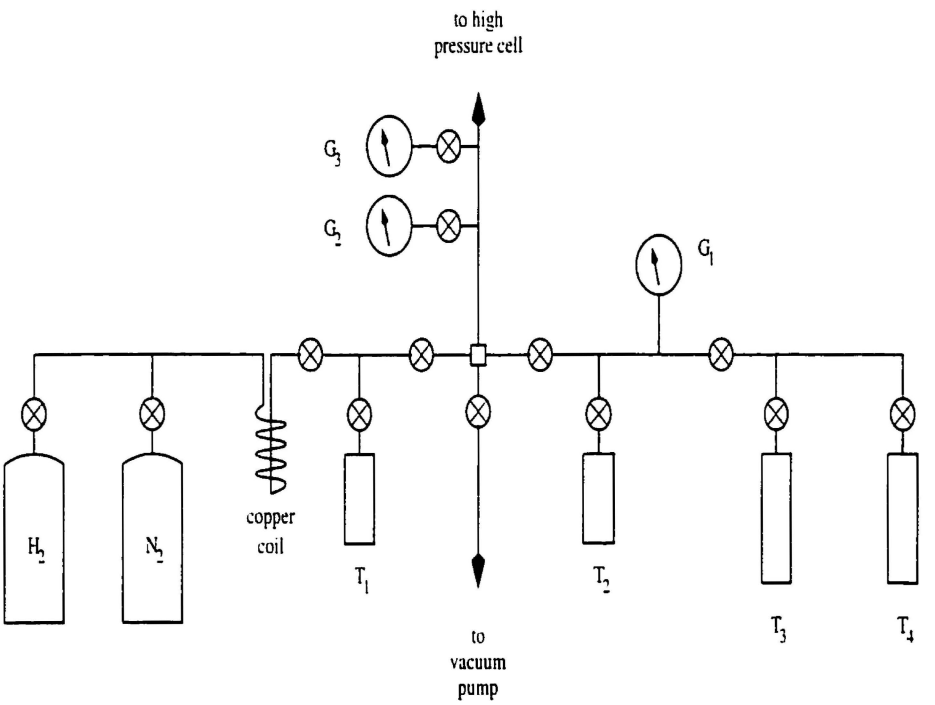


Figure 2.4: The high-pressure gas handling system. $T_1$ - $T_4$: thermal compressors; $G_1$, $G_2$, and $G_3$: Ashcroft-type Bourdon tube gauges.

## 2.5 Isothermal Data

The unit amagat is defined as the ratio of the density of a gas at a given temperature and pressure to the density of an ideal gas at standard temperature and pressure (S.T.P). If the density $\rho$ of a gas is expressed in units of amagat, then $\rho n_0$ is the number of gas molecules per $cm^3$ ($n_0$ being Loschmidt's number which is $2.687 \times 10^{19}$ $cm^{-3}$ for an ideal gas at STP) . The isothermal data were calculated from the tabulated PVT data for $H_2$[42] and $N_2$[43]. When necessary, linear interpolation was used to obtain the necessary temperature dependence, and a least-squares fit was used to determine the coefficients in the expression for density as a power series polynomial in pressure.

$$\rho = \sum_{i}^{O} a_i P^i, \tag{2.1}$$

where $a_i$ are the expansion coefficients, $\rho$ is the density in amagat, P the pressure in atm, and $O$ is the order of polynomial. The order was chosen by the standard method of testing using the $F$ statistic (see section A.2 in Appendix A) .

To calculate the partial densities of $N_2$ in a mixture with a fixed base density of $H_2$, the following method was used. First, the base density $\rho_{H_2}$ of $H_2$ was directly calculated from its known base pressure using the isothermal data fitted to equation 2.1. The partial density $\rho_{N_2}$ of $N_2$ was then calculated using the following formula[31]:

$$\rho_b = [1/(1+\beta')][(\rho_a)_P + \beta'(\rho_b)_P] - \rho_a \ , \tag{2.2}$$

where $(\rho_a)_P$ and $(\rho_b)_P$ are the densities of gas a (i.e., $H_2$) and b (i.e., $N_2$), respectively, at the total pressure P of the mixture, $\beta' = \rho_b'/\rho_a$, where $\rho_b'$ is the approximate partial density of gas b corresponding to the partial pressure $P_b = P - P_a$, $P_a$ being the partial pressure of gas a in the mixture. It is noted that $\rho_a + \rho_b$ represent the total density of the mixture.

Since equation 2.2 is nonlinear it lends itself to an iterative solution which converged when the difference between successive values of $\rho_b$ was smaller than $10^{-4}$ %. This convergence limit was set so much larger than the machine precision limit ( $10^{-13}$ % for double precision reals, which were used for all numerical calculations), because all such densities calculated would have uncertainties of $\approx$ 1 % anyway. To estimate this uncertainty in density (resulting from the uncertainty in the pressures readings from the gauges) the normal methods by differentials cannot be used on equation 2.2. Instead, one has to use the actual definition (see section A.7).

## 2.6 Method of Data Reduction

To determine the required absorption coefficients, the transmitted light intensities, $I_1(n)$ for the background, and $I_2(n)$ for a binary gas mixture, were recorded against the drum pulse number $n$ of the stepping motor, whose calibration is described in section 2.7. Other details of the intensities are given in section 3.1. Estimates of noise levels (standard errors described in section 2.3), $dI_1$ and $dI_2$, of the intensities were also recorded for each data set. Multiple data sets were recorded for each binary gas mixture and when necessary multiplicatively normalised (to account for a frequency independent intensity variation such as a drop in intensity of the lamp). This normalisation is accomplished by finding a parameter C that minimises the quantity

$$\sum_n \left( \frac{[I_i(n)/I_j(n)] - C}{\sigma(n)} \right)^2 . \tag{2.3}$$

Here $I_i(n)$ and $I_j(n)$ are two sample data sets for one particular binary gas mixture (or background) and $\sigma(n)$ is the uncertainty in $I_i(n)/I_j(n)$, and is calculated by the expression

$$\sigma(n) = \sqrt{\left(\frac{dI_i}{I_i(n)}\right)^2 + \left(\frac{dI_j}{I_j(n)}\right)^2}. \tag{2.4}$$

The parameter $C$ in equation 2.3 is the weighted average of the $I_i(n)/I_j(n)$ values with the weights being $1/\sigma(n)^2$, and the uncertainty in $C$ is the standard error[44] of the weighted average. A weighted average of these normalised data sets was calculated along with the standard error (which is now dependent on drum number). The required absorption coefficients were then calculated using equation 3.6 along with the uncertainty given by

$$d\alpha(n) = \sqrt{\left[\frac{dI_1(n)}{I_1(n)}\right]^2 + \left[\frac{dI_2(n)}{I_2(n)}\right]^2}. \tag{2.5}$$

which comes from standard error propagation methods[44] on equation 3.6 This uncertainty is less than 1 % .

The relative deviations $(I_i - I_jC)/I_j$ are minimised rather than the more natural absolute deviations ( $I_i - I_jC$ ) because the minimisation of the absolute deviations is much more complex. Its solution has to be obtained by a nonlinear least-squares method as opposed to the much simpler linear least-squares method described above to minimise the relative deviations. To use the absolute deviations one would solve the problem of fitting a straight line with zero intercept with uncertainties in both the dependent and independent variables. While this is possible[45], the slight gain in physical meaning is not worth the computational effort.

## 2.7 Calibration of the Spectral Region

The drum attached to the stepping motor was calibrated by recording two spectra in the spectral region 3000 to 10000 $cm^{-1}$. For the first spectrum the optical path was not flushed with nitrogen gas so that the atmospheric water vapour absorption lines would be present in the spectrum with high intensity, and for the second spectrum a mercury

lamp was used as the source to obtain the standard Hg emission lines. The standard wavenumbers $\nu$ of the water vapour absorption peaks[46] and those of the mercury emission lines[47] were plotted against the measured drum pulse number to insure a smooth functional dependence. Once this was verified a least-squares fit was used to determine the coefficients in the expression for wavenumber $\nu$ as a power series polynomial in drum number, given by

$$\nu(n) = \sum_{i}^{O} b_i n^i, \tag{2.6}$$

where $b_i$ are the expansion coefficients, and $O$ is the order of the polynomial which was chosen by the standard method of testing using the $F$ statistic (see section A.2) . The coefficients thus obtained allowed the calibration of the entire spectral region studied with an rms deviation less than 0.1 % . Since this is an order of magnitude less than the intensity error, it can be approximated as an exact calculation, which is a very important detail as uncertainties in the dependent variable will extremely complicate any analysis[45]. After the drum was calibrated, additional calibration spectra (using the mercury lamp once again as a source) were recorded after each set of spectra obtained for a particular binary gas mixture. The Hg emission lines in these calibration spectra were used to insure that the CIA spectra were aligned with initial calibration. Alternately, water vapour lines could also be used for alignment if they are present in the spectra.

# Chapter 3

# Theoretical Considerations

## 3.1 Absorption Coefficient

The absorption coefficient $\alpha(\nu)$ of a given gas at a particular wavenumber $\nu$ (in $cm^{-1}$) is generally represented by

$$I(\nu) = I_0(\nu)e^{-\alpha(\nu)l}, \tag{3.1}$$

where $I_0(\nu)$ is the intensity of the source, $I(\nu)$ is the transmitted intensity by a cell of sample path length $l$ containing a gas at a given density. In collision-induced absorption spectra if collisions of type $a - a$ are considered, equation 3.1 can be represented by

$$I_1(\nu) = I_0(\nu)e^{-\alpha_{aa}(\nu)l} . \tag{3.2}$$

In an experiment involving a binary gas mixture of gases a (e.g., $H_2$) and b (e.g., $N_2$) , equation 3.2 can be modified as

$$I_2(\nu) = I_0(\nu)e^{-[\alpha_{aa}(\nu)+\alpha_{ab}(\nu)+\alpha_{bb}(\nu)]l}, \tag{3.3}$$

or

$$I_2(\nu) = I_1(\nu)e^{-[\alpha_{ab}(\nu)+\alpha_{bb}(\nu)]l}, \tag{3.4}$$

where $\alpha_{aa}(\nu)$, $\alpha_{ab}(\nu)$, and $\alpha_{bb}(\nu)$ are absorption coefficients arising from collisions of types $a - a$, $a - b$, and $b - b$, respectively. If $\alpha_{bb}(\nu)$ is negligible in the spectral region of the

double vibrational transitions of $H_2$ ($v = 1 \leftarrow 0$) + $N_2$ ($v = 1 \leftarrow 0$), equation 3.4 can be simplified to

$$I_2(\nu) = I_1(\nu)e^{-\alpha_{ab}(\nu)l} \ . \tag{3.5}$$

which gives

$$\alpha_{ab}(\nu) = (1/l)\ln[I_1(\nu)/I_2(\nu)] \ . \tag{3.6}$$

The absorption coefficient $\alpha_{ab}(\nu)$ in equation 3.6 can be calculated theoretically by summing over all possible induction mechanisms, $L$, and all possible molecular transitions, $m$. Thus

$$\alpha_{ab}(\nu) = \sum_{Lm} \alpha_{ab,Lm}(\nu) \ . \tag{3.7}$$

Since in the current system there is no evidence of overlap absorption in the spectral region of interest only quadrupolar induction is considered to account for the absorption. Therefore equation 3.7 is reduced to

$$\alpha_{ab}(\nu) = \sum_{m} \alpha_{ab,m}(\nu). \tag{3.8}$$

## 3.2 Integrated Dimensionless Absorption Coefficient

The frequency dependence of the absorption coefficient, $\alpha(\nu)$, or the commonly defined, dimensionless absorption coefficient , $\tilde{\alpha}(\nu) = \alpha(\nu)/\nu$, cannot be expressed theoretically (except for the simplest systems, see section 3.6). However, the integrated dimensionless absorption coefficient $\tilde{A}$ ($=\int \tilde{\alpha}(\nu)d\nu$) is much more theoretically tractable and has been the focus of considerable theoretical work. At low densities where binary collisions

are predominant it is proportional to the product of the partial densities of the individual gases a and b of a binary mixture. So for given types of collisions the integrated dimensionless absorption coefficient can be expressed as

$$\tilde{A}_{Lm} = \int \tilde{\alpha}_{Lm}(\nu)d\nu = \tilde{A}_{ab,Lm}\rho_a\rho_b. \tag{3.9}$$

The proportionality constant $\tilde{A}_{ab,Lm}$ termed as the binary absorption coefficient in equation 3.9 can be calculated theoretically, and is written for multipole induction as[48, 49, 4]

$$\tilde{A}_{ab,Lm} = \frac{4\pi^3\nu_0^2e^2}{3ch}a_0{}^5(a_0/\sigma)^{2L+1}\tilde{J}_L X_{Lm}, \tag{3.10}$$

where

$$\tilde{J}_L = 4\pi(L+1)\int_0^\infty x^{-2(L+2)}g_0(x)x^2dx, \tag{3.11}$$

$$\begin{aligned} X_{Lm} = P_{J_1}P_{J_2} \quad [ \quad & C(J_1L_1J'_1;00)^2 < v_1J_1|Q_{L_1}|v'_1J'_1 >^2 \\ & C(J_20J'_2;00)^2 < v_2J_2|\alpha_2|v'_2J'_2 >^2 + \\ & C(J_2L_2J'_2;00)^2 < v_2J_2|Q_{L_2}|v'_2J'_2 >^2 \\ & C(J_10J'_1;00)^2 < v_1J_1|\alpha_1|v'_1J'_1 >^2] + Y_{Lm}, \end{aligned} \tag{3.12}$$

and

$$\begin{aligned} Y_{Lm} = P_{J_1}P_{J_2} \quad [ \quad & C(J_1LJ'_1;00)^2C(J_22J'_2;00)^2 \\ & \text{x } \frac{2}{9} < v_1J_1|Q_{L_1}|v'_1J'_1 >^2 < v_2J_2|\gamma|v'_2J'_2 >^2 + \\ + \quad & C(J_12J'_1;00)^2C(J_2LJ'_2;00)^2 \\ & \text{x } \frac{2}{9} < v_2J_2|Q_{L_2}|v'_2J'_2 >^2 < v_1J_1|\gamma|v'_1J'_1 >^2 \end{aligned}$$

$$
\begin{aligned}
- \quad & \frac{4}{15} C(J_1 2 J'_1; 00)^2 C(J_2 2 J'_2; 00)^2 \\
& \mathrm{x} < v_1 J_1 | Q_{L_1} | v'_1 J'_1 >^2 < v_2 J_2 | \gamma_2 | v'_1 J'_2 >^2 \\
& \mathrm{x} < v_2 J_2 | Q_{L_2} | v'_2 J'_2 >^2 < v_1 J_1 | \alpha_1 | v'_1 J'_1 >^2 ]. \qquad (3.13)
\end{aligned}
$$

In these equations, $L$ takes values 2,4,6, etc., for quadrapole ($2^2$), hexadecapole ($2^4$), tetrahexadecapole ($2^6$) induction, etc., ; $a_0$ is the first Bohr radius; $g_0(x)$ is the pair correlation function for the gas and $x = R/\sigma$, where $R$ is the intermolecular separation and $\sigma$ is the intermolecular separation at potential V(0)=0; subscripts 1 and 2 refer to the two colliding molecules; and $< |Q| > .< |\alpha| >$ , and $< |\gamma| >$ are the matrix elements of the $2^L$-pole induction, isotropic and anisotropic polarizability, respectively. The normalised Boltzmann factors $P_J$ are given by

$$
P_J = \frac{g_T(2J+1)e^{-E_J/kT}}{\sum_J g_T(2J+1)e^{-E_J/kT}} \; . \qquad (3.14)
$$

where $g_T$ is the nuclear statistical weight of the molecule in a given rotational state and $E_J$ is the rotational energy. For the even and odd J values $g_T$ takes values 1 and 3 for $H_2$, and 6 and 3 for $N_2$. The quantities $C(JLJ';00)$ are Clebsch-Gordan coefficients and their squares for the O ($\Delta J = -2$), Q ($\Delta J = 0$), and S ($\Delta J = +2$), transitions are given by the following equations[50] :

$$
\begin{aligned}
Q \; &: \; C(JJ';00)^2 = \delta_{JJ'} \\
O \; &: \; C(J2J-2;00)^2 = \frac{3J(J-1)}{2(2J-1)(2J+1)} \\
Q \; &: \; C(J2J;00)^2 = \frac{J(J+1)}{(2J-1)(2J+3)} \\
S \; &: \; C(J2J+2;00)^2 = \frac{3(J+1)(J+2)}{2(2J+1)(2J+3)} \; . \qquad (3.15)
\end{aligned}
$$

The intensities for the required transitions are calculated from the equations given above and the matrix elements of $H_2^{[51]}$.

## 3.3 Density Expansion of the Dimensionless Integrated Absorption Coefficient

If binary and higher order collisions are considered, equation 3.9 can be expanded as

$$\begin{aligned}\int \tilde{\alpha}(\nu)d\nu \;=\; & \tilde{A}_{ab}\rho_a\rho_b + \\ & \tilde{A}_{a2b}\rho_a{\rho_b}^2 + \tilde{A}_{2ab}{\rho_a}^2\rho_b + \\ & \tilde{A}_{a3b}\rho_a{\rho_b}^3 + \tilde{A}_{2a2b}{\rho_a}^3\rho_b + \tilde{A}_{3ab}{\rho_a}^2{\rho_b}^2 + \ldots \end{aligned} \tag{3.16}$$

where $\tilde{A}_{ab}$ is the binary absorption coefficient arising from collisions of type $a-b$, $\tilde{A}_{a2b}$ and $\tilde{A}_{2ab}$ are the ternary absorption coefficients arising from collisions of types $a-b-b$ and $a-a-b$, respectively, and $\tilde{A}_{a3b}$, $\tilde{A}_{2a2b}$, and $\tilde{A}_{3ab}$ are the quaternary binary absorption coefficient's arising from collisions of types $a-b-b-b$, $a-a-b-b$, and $a-a-a-b$, respectively.

## 3.4 Spectral Moments

The $n^{th}$ spectral moment $m_n$ is defined as ($\omega = 2\pi c\nu$)

$$m_n = \int_{-\infty}^{\infty} \omega^n W(\omega)d\omega \quad .n = 0, 1, 2, \ldots . \tag{3.17}$$

Here $W(\omega)$ is the spectral function. The spectral moments are also related to the time correlation function $C^n(t)$ by the following relation[11]

$$m_n = 2\pi i^{-n} C^n(t), \tag{3.18}$$

where $C^n(t)$ is the $n^{th}$ time derivative of the correlation function (which is simply the inverse Fourier transform of the spectral function $W(\omega)$). The spectral moments are of great utility when the region being studied is free from superposition from nearby bands. In such a case these can be usually expressed as simple functions of the lineshape parameters[11] and thus provide an efficient means to calculate the spectral parameters without fitting the experimental profile to a lineshape. This fitting is much more complex than the calculation represented by equation 3.17. The lineshape used in the present work (see section 3.5) does not have closed form expressions for the moments. This, however, does not impede analysis in the absorption profiles presented in this thesis, because the region has considerable overlap from neighbouring bands which makes lineshape analysis essential in order to separate the overlapping bands.

## 3.5 Lineshape Functions

The frequency dependence of the dimensionless absorption coefficient, $\tilde{\alpha}(\nu)$, can be modeled by a number of semi-empirical lineshapes $[W(\Delta\nu)]$. If the lineshapes do not inherently satisfy detailed balance and we introduce the following equation for $\alpha_{Lm}$ :

$$\tilde{\alpha}_{Lm}(\nu) = \tilde{A}_{Lm}\frac{NW(\Delta\nu)}{1+\exp(-hc\Delta\nu/kT)} \ . \tag{3.19}$$

where $\tilde{A}_{Lm} = \int \tilde{\alpha}_{Lm}(\nu)d\nu$, $N$ is the normalization factor, $\Delta\nu = \nu - \nu_m + \nu_s$, where $\nu_m$ is the wavenumber of a particular transition, and $\nu_s$ accounts for any perturbation in the molecular wavenumbers $\nu_m$, and the factor $1+\exp(-hc\Delta\nu/kT)$ satisfies the detailed balance condition. In order to calculate the total dimensionless absorption coefficient, the sum specified in equation 3.7 must be evaluated .

Several lineshapes have been used in the past to study the quadrupolar transitions which are of interest in the present experiment. First is the dispersion-type function

which is represented by

$$W_q(\Delta\nu) = 1/[1 + (\Delta\nu/\delta_q)^2], \tag{3.20}$$

where $\delta_q$ is the half-width at half height of the line. Gillard et al[52] represented the quadrupolar transitions in the CIA spectra of the fundamental band of $D_2$ at 77 K with a modified dispersion lineshape function given by

$$W_q(\Delta\nu) = 1/[1 + (\Delta\nu/\delta_2)^2 + (\Delta\nu/\delta_4)^4], \tag{3.21}$$

where $\delta_2$ and $\delta_4$ are the parameters of the lineshape. (See also Reddy et. al.[53], and Lewis and Tjon[54] for further details on this lineshape function.)

Birnbaum and Cohen[39] proposed a lineshape function which was first used in the analysis of the pure rotational spectrum of $H_2$. It can be written as

$$W_{BC}(\Delta\nu) = \frac{\tau_1}{\pi}\exp(\frac{\tau_2}{\tau_1})\exp(\frac{hc\Delta\nu}{2kT})\frac{zK_1(z)}{1 + (2\pi c\Delta\nu\tau_1)^2}\ , \tag{3.22}$$

where

$$z = [1 + (2\pi c\Delta\nu\ \tau_1)^2]^{1/2}[(\frac{\tau_2}{\tau_1})^2 + (\frac{h}{4\pi kT\tau_1})^2]^{1/2}. \tag{3.23}$$

where $K_1(z)$ is a modified Bessel function of the second kind of order 1 and $\tau_1$ and $\tau_2$ are characteristic times in the dipole moment correlation function. Wavenumber parameters $\delta_1$ and $\delta_2$ can also be used by defining $\delta_i = 1/2\pi c\tau_i$. Then $W_{BC}(\Delta\nu)$ and $z$ become

$$W_{BC}(\Delta\nu) = \frac{1}{2\pi^2 c\delta_1}\exp(\frac{\delta_1}{\delta_2})\exp(\frac{hc\Delta\nu}{2kT})\frac{zK_1(z)}{1 + (\Delta\nu/\delta_1)^2}, \tag{3.24}$$

and

$$z = [1 + (\Delta\nu/\delta_1)^2]^{1/2}[(\frac{\delta_1}{\delta_2})^2 + (\frac{hc\delta_1}{2\pi kT})^2]^{1/2}. \tag{3.25}$$

Since the BC lineshape inherently satisfies detailed balance, equation 3.19 is modified to

$$\tilde{\alpha}_{Lm}(\nu) = \tilde{A}_{Lm}.VW(\Delta\nu) \ . \tag{3.26}$$

The lineshape function which consistently gave the best results in the systems studied here was recently developed by Lewis[38] and is a modification of the Birnbaum-Cohen lineshape. It is referred to as the Lewis-Birnbaum-Cohen (LBC) lineshape which is given by

$$W_{LBC}(\Delta\omega) = \frac{2}{1 + e^{-\beta\hbar\Delta\omega}} \frac{e^{\tau_2/\tau_1}}{\pi} \frac{\tau_2}{\sqrt{1 + \Delta\omega^2\tau_1^2}} K_1(\frac{\tau_2}{\tau_1}\sqrt{1 + \Delta\omega^2\tau_1^2}). \tag{3.27}$$

Here $K_1$ is the same as defined in equation 3.22, and $\Delta\omega = \omega - \omega_m + \omega_s$ where $\omega_m$ is the frequency of the m'th transition. The LBC lineshape is derived from a slight modification of the procedure used in developing the Birnbaum-Cohen (BC) lineshape[39] . The same time correlation function is used in both; however, the LBC lineshape uses Boltzmann asymmetrization to satisfy detailed balance and the BC lineshape uses Egelstaff time[55]. Both lineshapes are used for the analysis of spectra containing many induced transitions.

To model the frequency dependence of the dimensionless absorption coefficient as determined by the present experimental data it was necessary to slightly modify equation 3.26 as

$$\tilde{\alpha}_{Lm}(\nu) = \tilde{A}_{Lm}SNW(\Delta\nu) + B/\nu, \tag{3.28}$$

where $S$ accounts for any necessary multiplicative correction to the theoretical value of the integrated absorption $\tilde{A}_{Lm}$, whereas $B$ accounts for any frequency independent difference between the background spectrum and binary gas mixture absorption spectrum.

Thus there are five adjustable parameters in the model being fitted to the data. The LBC lineshape has three adjustable parameters: $\tau_1$, which mainly determines line width; $\tau_2$, which mainly determines how fast the tail falls off; and $\omega_s$ which accounts for any perturbation in the transition frequencies. In the fitting it was necessary to approximate $\tilde{A}_{Lm}$ using equation 3.9. This approximation is valid in the present set of experiments as only binary absorption was significant. It is to be noted that in the equations 3.26 and 3.28 , $W(\Delta\nu)$ stands for either $W_{BC}(\Delta\nu)$ or $W_{LBC}(\Delta\nu)$. In equations 3.19 , 3.26, and 3.28, the normalization factor N is defined such that equation 3.9 holds.

## 3.6 Quantum Lineshapes

Aside from the empirical lineshapes like $W_{BC}(\Delta\nu)$ and $W_{LBC}(\Delta\nu)$, there exist quantum lineshapes[56] that do not contain any floated parameters and are derived from purely quantum mechanical considerations. These quantum lineshapes have so far only been used on relatively simple systems such as the CIA spectra of the 1-0 and 2-0 bands of $H_2$[57, 58] in the pure gas and the 1-0 band of $H_2$ in $H_2$-He[59] mixtures, and the 1-0 band of $N_2$[60]. Because of the significant increase in complexity and resulting computation required no quantum lineshape calculations have been performed to date on systems containing double vibrational transitions in binary mixtures.

# Chapter 4

## Absorption Spectra of Double Vibrational Transitions of $H_2$+$N_2$

### 4.1 Introduction

A brief survey of the previous work on the CIA spectra of $H_2$ and that of $N_2$, both in the gaseous phase, is given in Chapter 1. Details of the apparatus and experimental techniques are described in Chapter 2. Theoretical aspects and lineshape functions are summarized in Chapter 3. In the present research project the CIA spectra of the double vibrational transitions of $H_2$ ($v = 1 \leftarrow 0$) + $N_2$ ($v=1 \leftarrow 0$) in their binary mixtures were recorded at 201 and 298 K for a number of base gas densities of $H_2$ in $H_2$-$N_2$ mixtures. As these transitions overlap with the high wavenumber wing of the fundamental band of $H_2$ in $H_2 - N_2$ mixtures, a wider spectral region beyond the region of the double vibrational transitions was recorded for each of the gas mixtures used. As the absorption in each $H_2 - N_2$ mixture is obtained with reference to the absorption profile of the pure, $H_2$ gas, the contribution arising from the $H_2 - H_2$ collisions is removed. A method of profile analysis is used to separate the enhancement of absorption of the fundamental band of $H_2$ in $H_2 - N_2$ mixtures from the total absorption. The CIA in the first overtone region of $N_2$ ($v = 2 \leftarrow 0; v_1 = 1 \leftarrow 0 + v_2 = 1 \leftarrow 0$) in the pure gas occurs in the region 4200 - 5200 $cm^{-1}$ and has negligible absorption in the region of double vibrational transitions of present interest. A summary of the experimental conditions under which these spectra were recorded is given in Table 4.1. The experimental absorption profiles and their analysis are presented in the rest of this chapter.

Table 4.1: Summary of the experimental conditions

| Temperature (K) | Absorption path length (cm) | Base density of $H_2$ (amagat) | Range of partial densities of $N_2$ (amagat) |
|---|---|---|---|
| 201 | 185.5 | 305.0 | 70.3 - 207.8 |
| | | 351.9 | 100.3 - 204.1 |
| | | 387.9 | 85.2 - 209.5 |
| 298 | 185.8 | 135.6 | 90.0 - 366.4 |
| | | 185.6 | 85.9 - 305.0 |
| | | 209.4 | 80.2 - 271.2 |
| | | 171.5 | 128.6 - 211.3 |
| | | 258.8 | 130.3 - 252.9 |

## 4.2 Profiles of the CIA Fundamental Band of $H_2$ in the Pure Gas

Typical examples of CIA spectra of the fundamental band of $H_2$ in the pure gas recorded with the 2.0 m absorption cell at 77, 196 and 298 K for gas densities 43.4, 39.4, and 38.5 amagat respectively in the region 3800-5700 $cm^{-1}$, adopted from Reddy et. al.[25] (1977) are shown in figure 4.1. The positions of the 'single' transitions $O_1(J)$ $Q_1(J)$, and $S_1(J)$, calculated from the constants of the free molecule (see Figure 1.1) are shown along the wavenumber axis. The extent of the group of 'single' and double transitions are marked over the absorption peaks. Almost all molecules of $H_2$ are distributed among the rotational levels J=0 and 1 at 77 K and J=0 to 3 at 198 and 298 K. As seen in this figure, both the shape of the bands and the characteristic overlap dip in the Q branch with low and high wavenumber maximum denoted by $Q_P$ and $Q_R$ are dependent on temperature and density. The enhancement of absorption of the collision-induced-fundamental band of $H_2$ in $H_2 - N_2$ mixtures at much higher densities than those of the

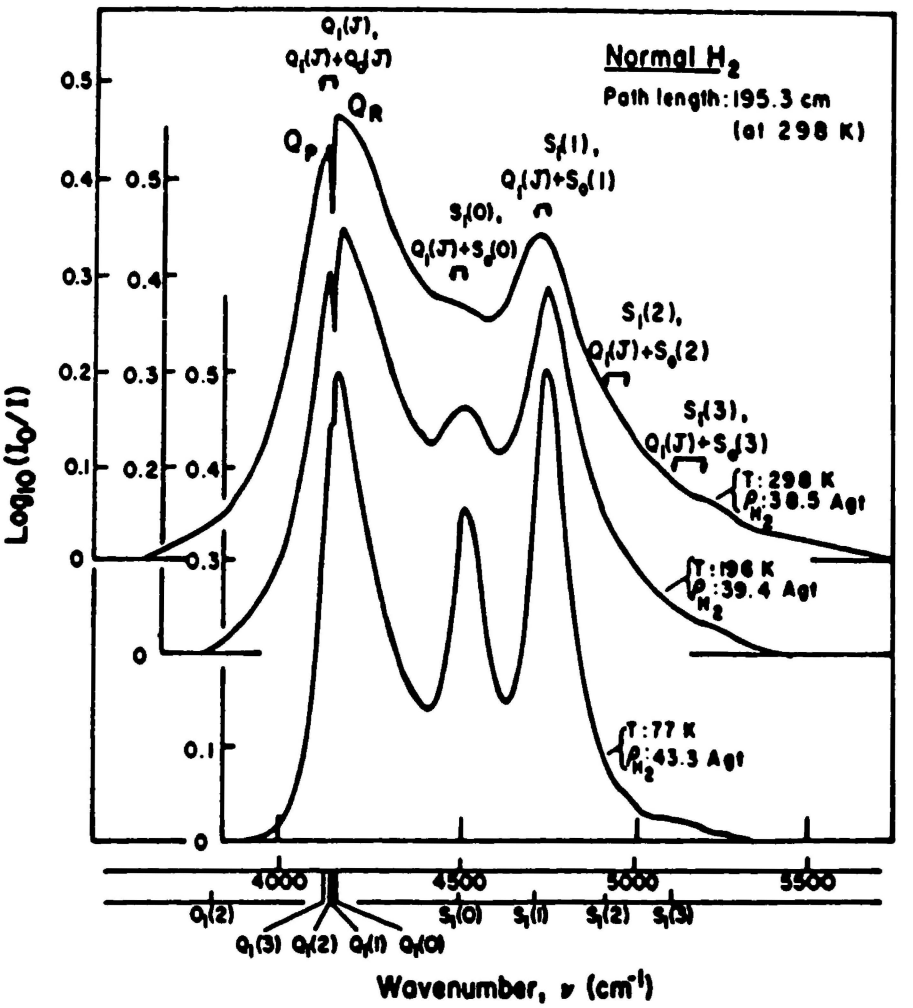


Figure 4.1: Absorption profiles of the fundamental band of $H_2$ in the pure gas at 77, 196 and 298 K.

profiles in Figure 4.1 extend to higher wavenumbers than 5700 $cm^{-1}$. As stated in Section 4.1, the enhancement of absorption of the fundamental band of $H_2$ in $H_2 - N_2$ mixtures is separated from the absorption of the double vibrational transitions $H_2$ ($v = 1 \leftarrow 0$) + $N_2$ ($v = 1 \leftarrow 0$) occurring in the region 5900-7400 $cm^{-1}$ by the method of profile analysis as shown later in this chapter.

## 4.3 Experimental Absorption Spectra of Double Vibrational Transition of $H_2 - N_2$

Three representative absorption profiles of double vibrational transitions $H_2$ (v'=1, J' $\leftarrow$ v=0,J) + $N_2$ (v'=1, J' $\leftarrow$ v=0,J) in three binary mixtures of $H_2$ and $N_2$ at each of the temperatures 201 and 298 K are shown in Figures 4.2, and 4.3, respectively. In these figures relative values of $(1/\rho_{H_2}\rho_{H_2})\tilde{\alpha}(\nu)$ are plotted against wavenumber in the spectral region 5900-7400 $cm^{-1}$. The absorption peaks in the figures are identified with numbers 1 to 6. The positions of the absorption peaks and the assignment of the double vibrational transitions $O_1(3) + Q_1(J)$ , $O_1(2) + Q_1(J)$ , $Q_1(J) + O_1(J)$ , $Q_1(J) + Q_1(J)$ , $Q_1(J) + S_1(J)$ , $S_1(0) + Q_1(J)$ , $S_1(1) + Q_1(J)$ , and $S_1(2) + Q_1(J)$ , are listed in Table 4.2 In these double transitions, the first one is from $H_2$ and the second one is from $N_2$. Unlike the characteristic dip in the Q branch of the fundamental band of $H_2$ (Figure 4.1), there is no evidence of it in the Q branch [i.e., $Q_1(J) + Q_1(J)$] around 6484 $cm^{-1}$. This implies that the overlap induction mechanism makes little or no contribution to the double fundamental transitions of $H_2$ and $N_2$. Thus it is justified to consider quadrupole induction mechanism only in the calculation of the intensities of the double fundamental transitions of $H_2 + N_2$.

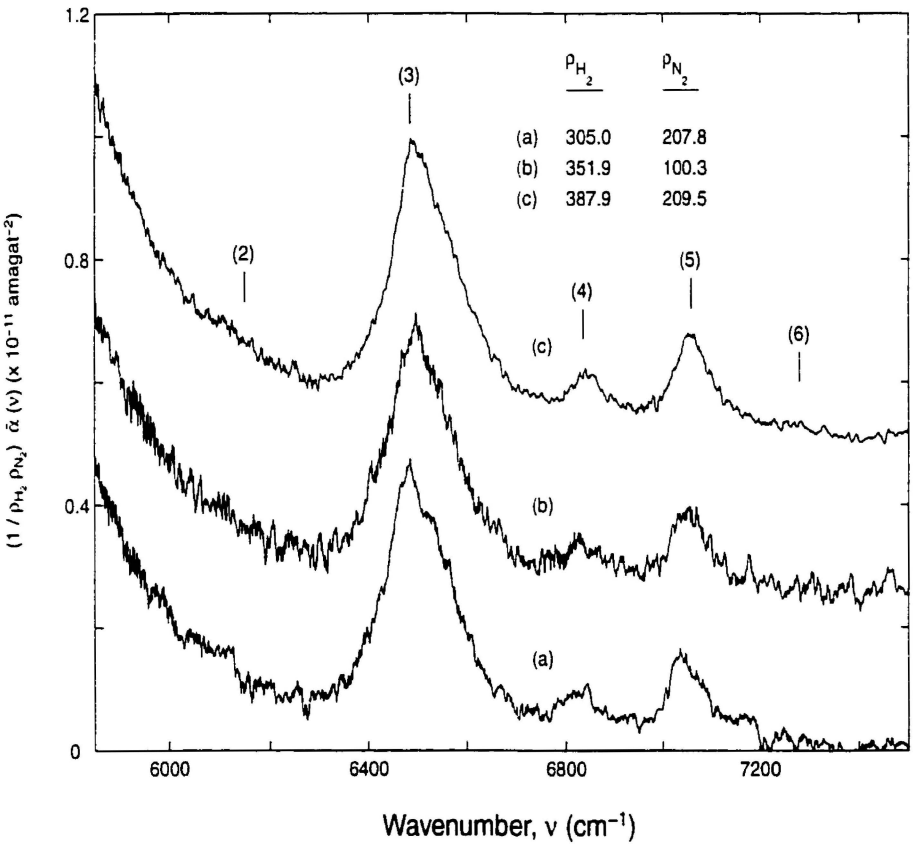


Figure 4.2: Collision-induced absorption profiles of the double vibrational transitions $H_2$ (v'=1, J' ← v=0,J) + $N_2$ (v'=1, J' ← v=0,J) in three binary mixtures of $H_2$ and $N_2$ at 201 K with a sample path length of 185.5 cm in the spectral region 5900 - 7400 $cm^{-1}$. The vertical axis represents relative absorption in the specified units. The assignments of the absorption peaks are given in Table 4.2. The given densities are in amagat units.

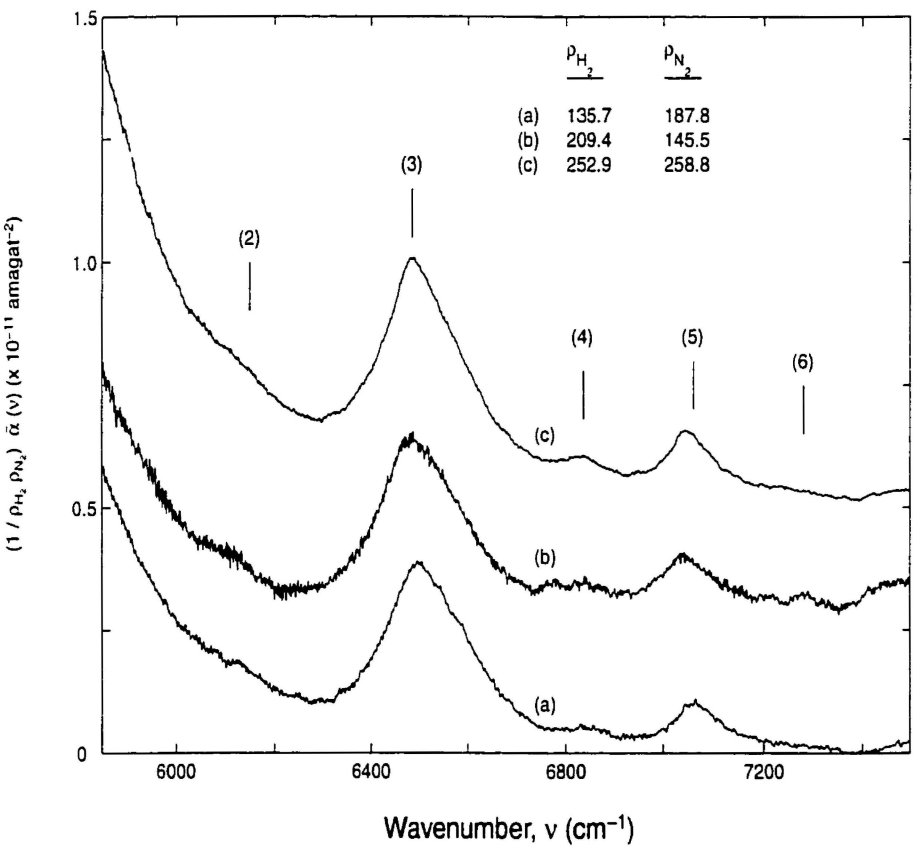


Figure 4.3: Caption for this figure in similar to the one for Figure 4.2 except that the profile in the figure are obtained at 298 K with a sample path length of 185.8 cm. The given densities are in amagat units.

Table 4.2: Absorption peak positions at 201 K and 298 K

| Absorption Peak | Position ($cm^{-1}$) | Transition ($H_2 + N_2$). |
|---|---|---|
| 1 | 5922 | $O_1(3) + Q_1(J)$ |
| 2 | 6149 | $O_1(2) + Q_1(J)$ |
| 3 | 6484 | $Q_1(J) + O_1(J)$<br>$Q_1(J) + Q_1(J)$<br>$Q_1(J) + S_1(J)$ |
| 4 | 6835 | $S_1(0) + Q_1(J)$ |
| 5 | 7060 | $S_1(1) + Q_1(J)$ |
| 6 | 7279 | $S_1(2) + Q_1(J)$ |

## 4.4 Integrated Binary Absorption Coefficient for Double Vibrational Transitions of $H_2 - N_2$

As stated in Chapter 3, the integrated binary absorption coefficient of a specific $L^{th}$ order multiple-induced transition in a binary gas mixture of component molecules a and b, following Reddy[4], is expressed as

$$\tilde{A}_{ab.Lm} = \frac{4\pi^3 n_0^2 e^2}{3ch} a_0{}^5 (a_0/\sigma)^{2L+1} \tilde{J}_L . X_{Lm} \ . \tag{4.1}$$

Equation (4.1) is the same as equation (3.10) in which $\tilde{J}_L$ and $X_{Lm}$ are given by equations (3.11) and (3.12), respectively. In the case of $H_2 - N_2$ double vibrational transitions the term $Y_{Lm}$ in equation (3.12) is neglected. In equation (4.1), $\tilde{J}_L$ is written as

$$\tilde{J}_L = 4\pi(L+1)\int_0^\infty x^{-2(L+2)} g_0(x) x^2 dx \ . \tag{4.2}$$

Assuming the quadrupole matrix elements $< |Q| >$ and isotropic polarizability matrix

elements $< |\alpha| >$ of $N_2$ are independent of the rotational quantum number $J$ unlike those of $H_2$. $X_{Lm}$ in equation (4.2) can be simplified as (from equation (3.12))

$$\begin{aligned} X_{Lm} = P_{J_1} P_{J_2} \; [ \; & C(J_1 L_1 J'_1; 00)^2 < v_1 J_1 | Q_{L_1} | v'_1 J'_1 >^2 \\ & C(J_2 0 J'_2; 00)^2 \alpha_2{}^2 + \\ & C(J_2 L_2 J'_2; 00)^2 Q_{L_2}{}^2 \\ & C(J_1 0 J'_1; 00)^2 < v_1 J_1 | \alpha_1 | v'_1 J'_1 >^2 ] \; . \end{aligned} \tag{4.3}$$

In these equations, $L = 2$ for quadrupole ($2^2$), $a_0$ is the first Bohr radius, $g_0(x)$ is the pair correlation function for the gas and $x = R/\sigma$, where $R$ is the intermolecular separation and $\sigma$ is the intermolecular separation at potential V(0)=0; subscripts 1 and 2 refer to the two colliding molecules; and $< |Q_{L_1}| >$ and$< |\alpha_1| >$ are the matrix elements of the $2^L$-pole induction and isotropic polarizability, respectively. The normalised Boltzmann factors $P_J$ are given by equation (3.14) in which the nuclear statistical weight $g_T$ takes values 1 and 3 for $H_2$, and 6 and 3 for $N_2$ for even and odd $J$ values, respectively. The squares of the Clebsch-Gordan coefficients for the O, Q, and S, transitions are given by equation (3.15). The matrix elements of of $H_2$ are given by Hunt et. al.[51]. The relative integrated binary absorption coefficients for the double vibrational transitions at 201 and 28 K were calculated using the formula discussed above.

## 4.5 Lewis-Birnbaum-Cohen (LBC) Lineshape Function

Several semi-empirical lineshapes used in the analysis of the CIA spectra are discussed in Section 3.5 (equations 3.19, 3.20, and 3.21). Birnbaum-Cohen lineshape function $W_{BC}(\Delta\nu)$ used initially in the analysis of the pure rotation spectrum of $H_2$ is represented

by equations 3.22 and 3.23 in terms of the time parameters $\tau_1$ and $\tau_2$ which are characteristic times in the induced dipole moment correlation function. $W_{BC}$ can be also represented by the wavenumber parameters $\delta_1$ and $\delta_2$ ($\delta_i = 1/2\pi c\tau_i$) by equation (3.24).

The BC lineshape inherently satisfies the so-called detailed balance and the absorption coefficient $\tilde{\alpha}_{Lm}$ can be represented by equation 3.28 as

$$\tilde{\alpha}_{Lm}(\nu) = \tilde{A}_{Lm} N W(\Delta\nu) \ . \tag{4.4}$$

where $\tilde{A}_{Lm} = \int \tilde{\alpha}_{Lm}(\nu)d\nu$, $N$ is the normalization factor, $\Delta\nu = \nu - \nu_m + \nu_s$ where $\nu_m$ is the wavenumber of a particular transition, and $\nu_s$ accounts for any perturbation in the molecular wavenumbers $\nu_m$. Lewis[38] proposed a modification to the BC lineshape and the resulting lineshape is referred to as the Lewis-Birnbaum-Cohen lineshape (LBC) and is expressed as ($\omega = 2\pi c\nu$; $\Delta\omega = 2\pi c\Delta\nu$) (equation 3.27)

$$W_{LBC}(\Delta\omega) = \frac{2}{1+e^{-\beta\hbar\Delta\omega}} \frac{e^{\tau_2/\tau_1}}{\pi} \frac{\tau_2}{\sqrt{1+\Delta\omega^2{\tau_1}^2}} K_1\left(\frac{\tau_2}{\tau_1}\sqrt{1+\Delta\omega^2{\tau_1}^2}\right). \tag{4.5}$$

Here $K_1$ is a modified Bessel function of the second kind of order 1 and $\tau_1$ and $\tau_2$ are defined above. The LBC lineshape is derived from a slight modification of the procedure used in developing the BC lineshape. It is to be noted that the LBC lineshape uses Boltzmann asymmetrization to satisfy detailed balance whereas the BC lineshape uses Egelstaff time[55]. In the present work equation (4.5) is modified as

$$\tilde{\alpha}_{Lm}(\nu) = \tilde{A}_{Lm} S N W(\Delta\nu) + B/\nu, \tag{4.6}$$

where $S$ accounts for any necessary multiplicative correction to the integrated absorption coefficient $\tilde{A}_{Lm}$ and $B$ accounts for any frequency-independent difference between the background $H_2$ spectrum and $H_2 - N_2$ binary gas mixture spectrum. Thus there are five adjustable parameters in the model being fitted to the data. In the LBC lineshape $\tau_1$

and $\tau_2$ are adjustable parameters; $\tau_1$, mainly determines line width; $\tau_2$ accounts for how fast the tail falls off. In equation 4.6, $N$ is defined so that equation 3.9 is satisfied.

## 4.6 Profile Analysis and Results

Individual double vibrational transitions of $H_2$ + $N_2$ discussed in earlier sections and the transitions in the enhancement of the fundamental band of $H_2$ in $H_2$ – $N_2$ mixtures were represented by the Lewis-Birnbaum-Cohen (LBC) lineshape function $W_{LBC}$ given by equation (4.5) and the absorption coefficient $\tilde{\alpha}_{Lm}(\nu)$ is represented by equation 4.1. A superposition of the individual components of the enhancement spectrum of the $H_2$ fundamental band in $H_2+N_2$ and of those of the double vibrational transitions of $H_2+N_2$ was used to construct the synthetic absorption profiles in the spectral region 5900-7400 $cm^{-1}$. A nonlinear least-squares fitting computer program was used to fit the calculated profiles to the corresponding experimental profiles until most satisfactory agreement between them was achieved. The criterion for the best fit is represented by the $\chi^2$ statistic, given as

$$\chi^2 = \sum_{i}^{N} \left[ \frac{y_{calc}(i) - y_{obs}(i)}{\sigma(i)} \right]^2 . \tag{4.7}$$

where $y_{obs}(i)$ and $y_{calc}(i)$ are the observed and calculated datum, $\sigma(i)$ is the uncertainty and $N$ is the number of the observed data. Nonlinear least-squares fitting and other relevant statistics used in the present analysis are described in detail in Appendix A. The parameters used in the profile analysis are the time parameters $\tau_1$ and $\tau_2$, $S$, $B$, and the possible shift of the free molecular wavenumber $\nu_m$ .

Examples of the analyzed profiles of the absorption spectra at 201 and 298 K are shown in Figures 4.4 and 4.5, respectively. In these figures the experimental profile is represented by solid lines; the dots represent the calculated high wavenumber wing of the

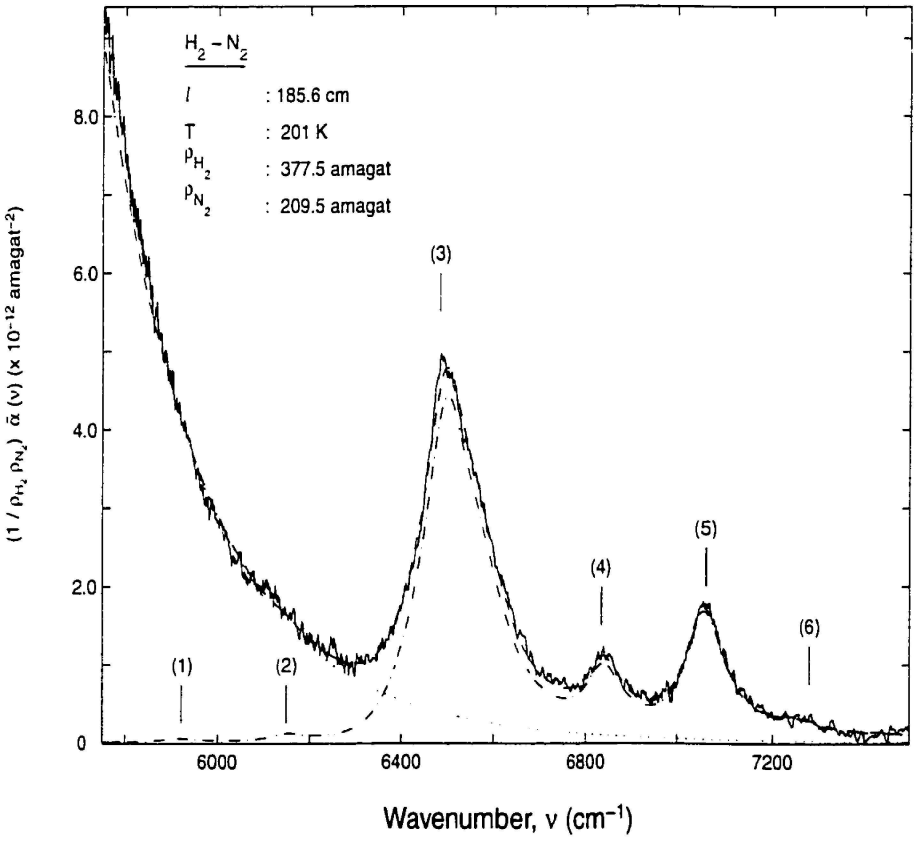


Figure 4.4: Analysis of an absorption profile of the double vibrational transitions of $H_2$ + $N_2$ at 201 K. The solid line (-) is the experimental profile. The dots (. . .) represent the synthetic high wavenumber wing of the enhancement of the CIA fundamental band of $H_2$ in a $H_2$+$N_2$ mixture. The dash-dot (- . -) curve represents the synthetic double vibrational transitions of $H_2$+$N_2$. The total synthetic profile is represented by the dashed (–) curve.

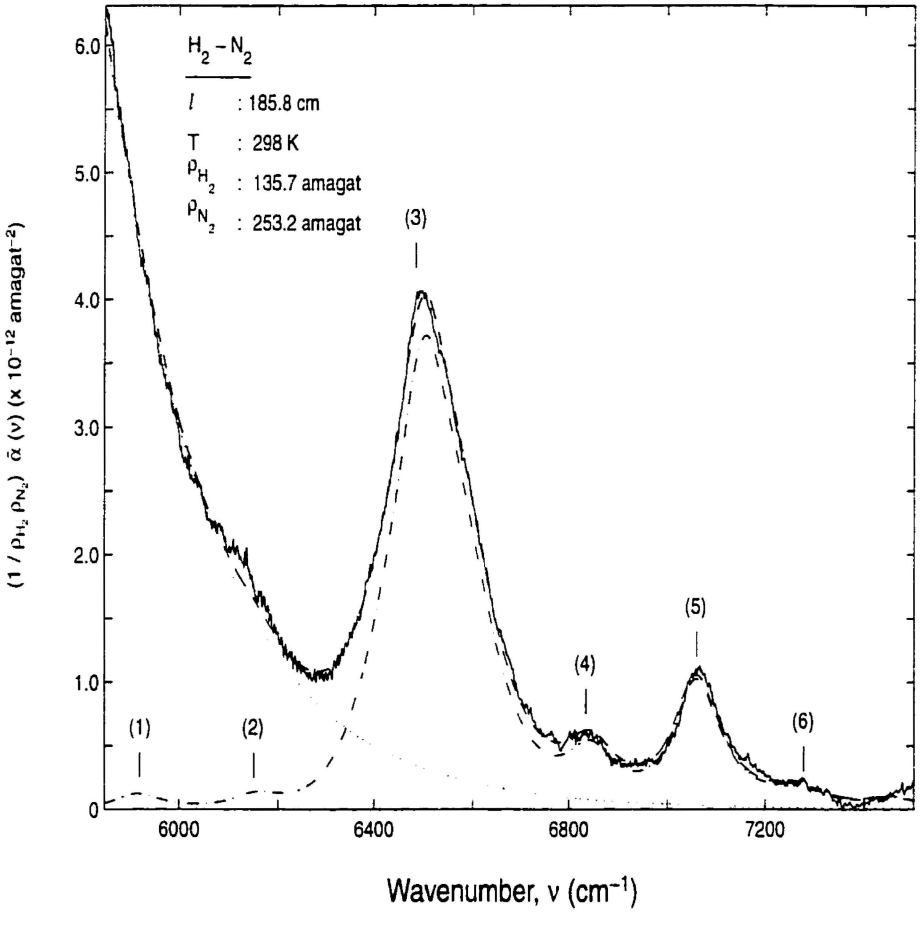


Figure 4.5: Caption for this figure in similar to the one for Figure 4.4 except that the profile in this figure is obtained at 298 K

Table 4.3: Linear dependence of $\tau_1$ and $\tau_2$

| Temperature (°K) | | Intercept ($s$) | Slope ($s\ cm^{-1}$) |
|---|---|---|---|
| 201 | $\tau_1$ | 0.97 ± 0.13 x $10^{-13}$ | 0.84 ± 0.65 x $10^{-16}$ |
| | $\tau_2$ | 0.42 ± 0.20 x $10^{-13}$ | -0.18 ± 0.15 x $10^{-15}$ |
| 298 | $\tau_1$ | 0.754 ± 0.098 x $10^{-13}$ | 0.46 ± 0.39 x $10^{-16}$ |
| | $\tau_2$ | 0.434 ± 0.086 x $10^{-13}$ | -0.110 ± 0.039 x $10^{-16}$ |

enhancement of the CIA fundamental band of $H_2$ in the $H_2$+$N_2$ mixture; the dash-dot curve represents the calculated double vibrational transitions of $H_2$+$N_2$; and the dashed curve is the total calculated profile. As is seen from these figures that the agreement between the experimental and the total calculated profile at each temperature is very good in the entire region of interest.

Plots of $\tau_1$ and $\tau_2$ against $\rho_{N_2}$, partial density of nitrogen in the mixture of $H_2$ + $N_2$ for 11 absorption profiles at 201 K are shown in Figures 4.6 and 4.7, respectively. Similar plots for 27 absorption profiles obtained at 298 K are shown in Figures 4.8 and 4.9 . It is evident from Figures 4.6 and 4.8 that $\tau_1$ $(= 1/2\pi c\delta_1)$ increases linearly with $\rho_{N_2}$ indicating a definite trend of "narrowing" of $\delta_1$ (the characteristic half-width parameter) with increasing partial density of nitrogen, $\rho_{N_2}$. It is to be pointed out here that in the CIA spectra of the fundamental band of $H_2$ in $H_2$-Ar, $H_2$-Kr, and $H_2$-Xe similar pressure narrowing has been reported by De Remigis et. al.[29] (1971) and Mactaggart et. al.[30] (1973) for densities higher than 300 amagat of the foreign gas. In the present work, the secondary parameter $\tau_2$ also shows a linear dependency on $\rho_{N_2}$ at 201 and 298 K as shown in Figures 4.7 and 4.9, respectively. The linear parameters for this dependence is given in Table 4.3 .

From the analyzed absorption profiles, the areas under the calculated profiles of the

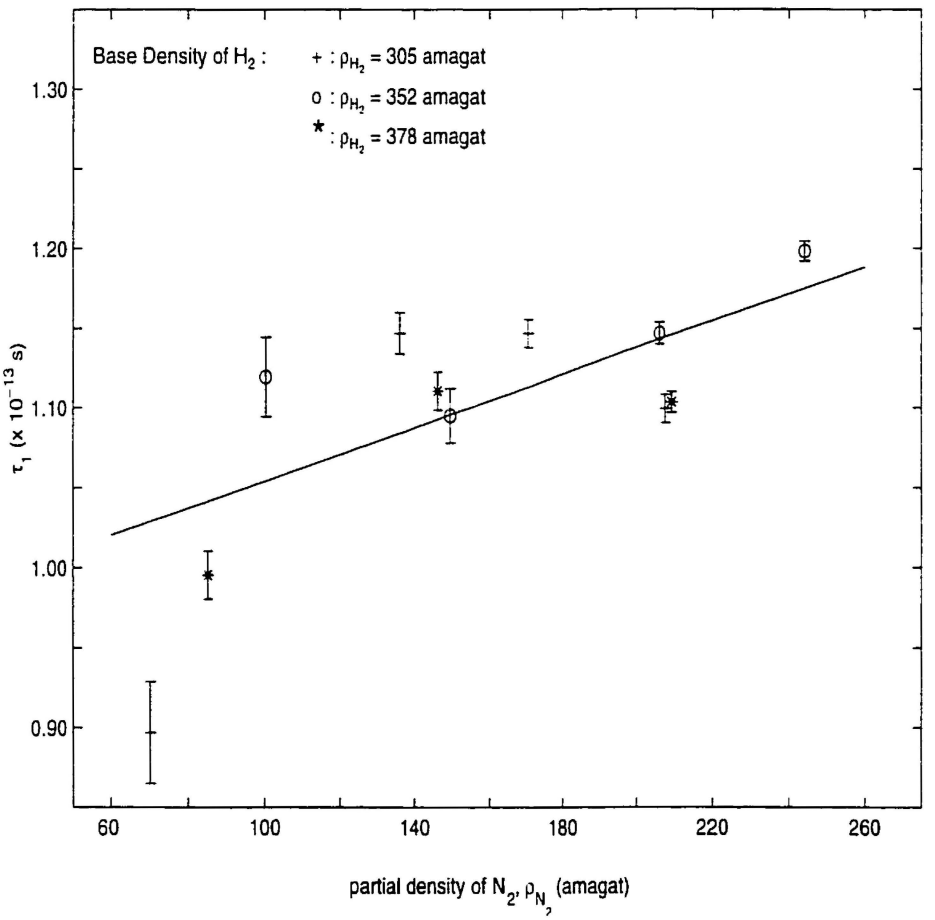


Figure 4.6: A plot of the parameter $\tau_1$ as a function of partial density of nitrogen $\rho_{N_2}$ at 201 K.

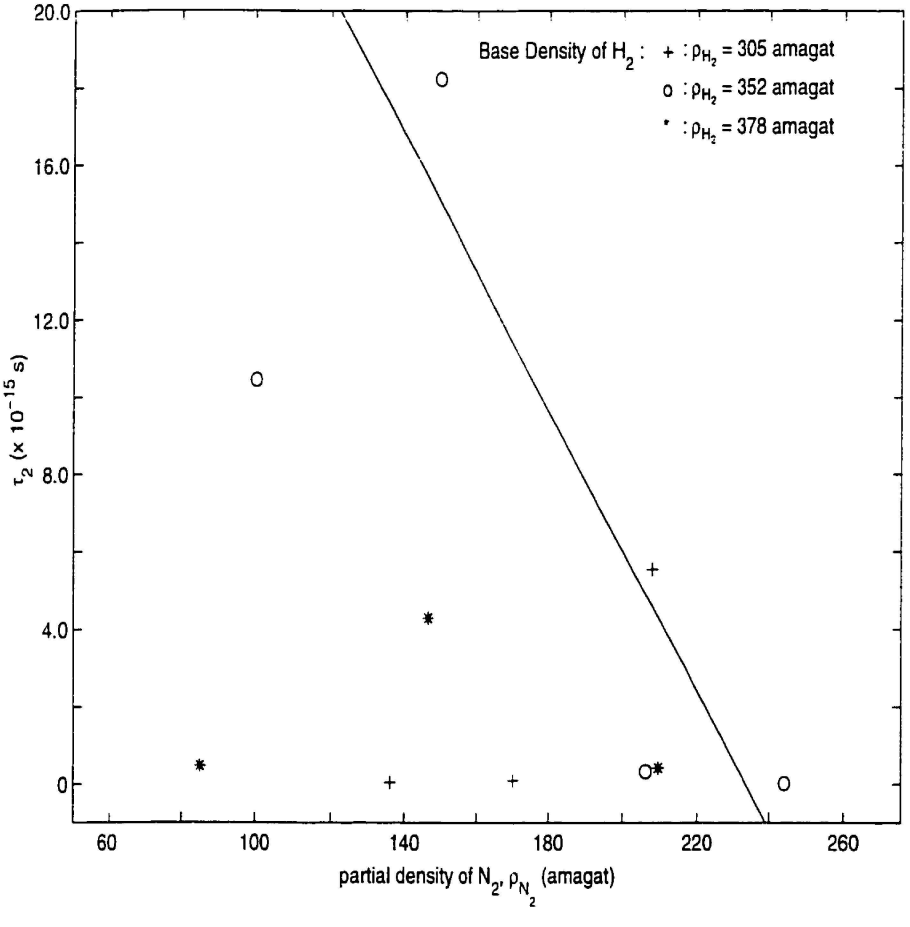


Figure 4.7: A plot of the parameter $\tau_2$ as a function of partial density of nitrogen $\rho_{N_2}$ at 201 K.

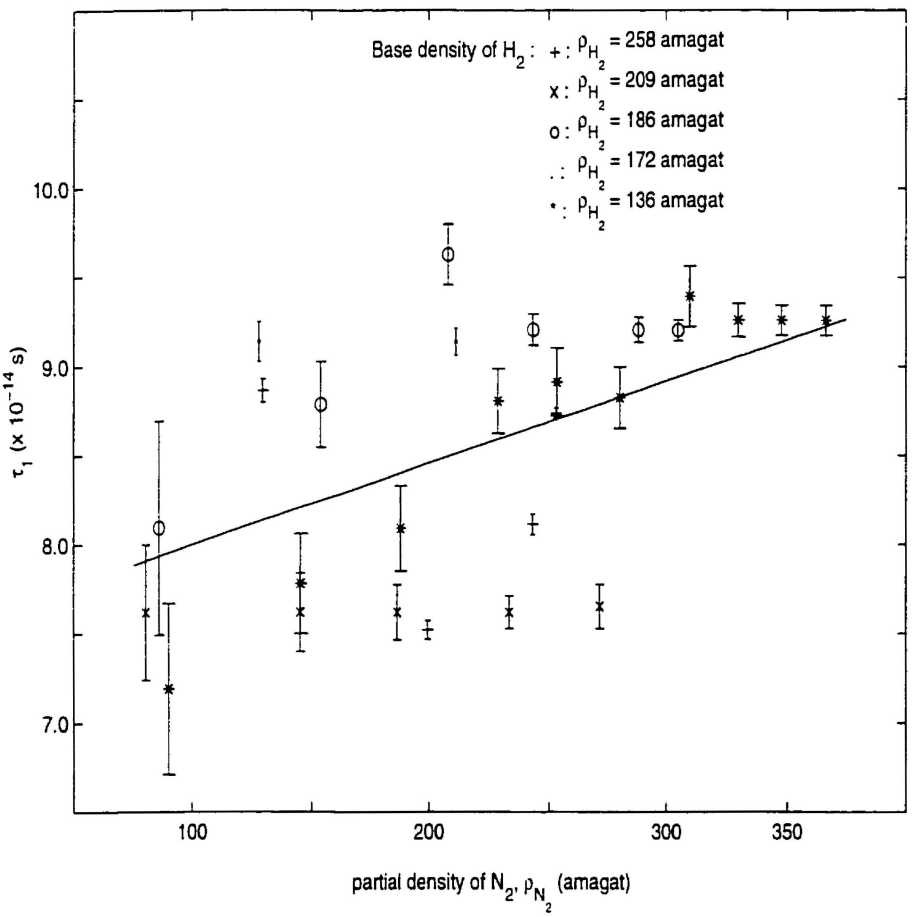


Figure 4.8: A plot of the parameter $\tau_1$ as a function of partial density of nitrogen $\rho_{N_2}$ at 298 K.

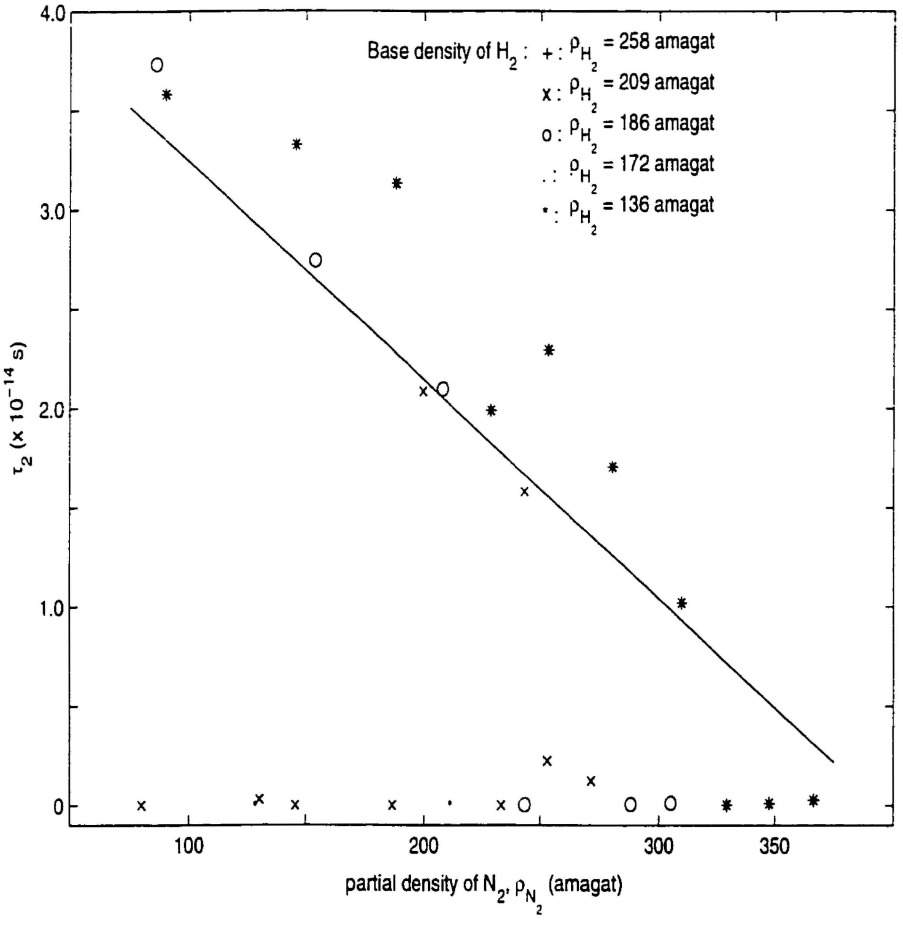


Figure 4.9: A plot of the parameter $\tau_2$ as a function of partial density of nitrogen $\rho_{N_2}$ at 298 K.

Table 4.4: Absorption Coefficient

| Temperature (K) | Binary Absorption coefficient $\tilde{A}_{ab}$ ($cm^{-1}$ $amagat^{-2}$) | Ternary Absorption coefficient $\tilde{A}_{a2b}$ ($cm^{-1}$ $amagat^{-3}$) |
|---|---|---|
| 201 | 0.101 ± 0.014 x $10^{-8}$ | 0.109 ± 0.076 x$10^{-11}$ |
| 298 | 0.104 ± 0.022 x $10^{-8}$ | 0.107 ± 0.085 x$10^{-11}$ |

double vibrational transitions, i.e., $(1/\rho_{H_2}\rho_{N_2}) \int \tilde{\alpha}(\nu)$ are plotted against $\rho_{N_2}$ for 201 and 298 K in Figures 4.10 and Figure 4.11, respectively. These plots show linear relationships with positive slopes. These can be represented by the linear equation

$$(1/\rho_a\rho_b) \int \tilde{\alpha}(\nu)d\nu = \tilde{A}_{ab} + \tilde{A}_{a2b}\rho_a\rho_b. \tag{4.8}$$

where these symbols have the same meaning as in equation 3.16. The values of $\tilde{A}_{ab}$ and $\tilde{A}_{a2b}$ resulting from the fits in Figures 4.11, 4.11 are given in Table 4.4.

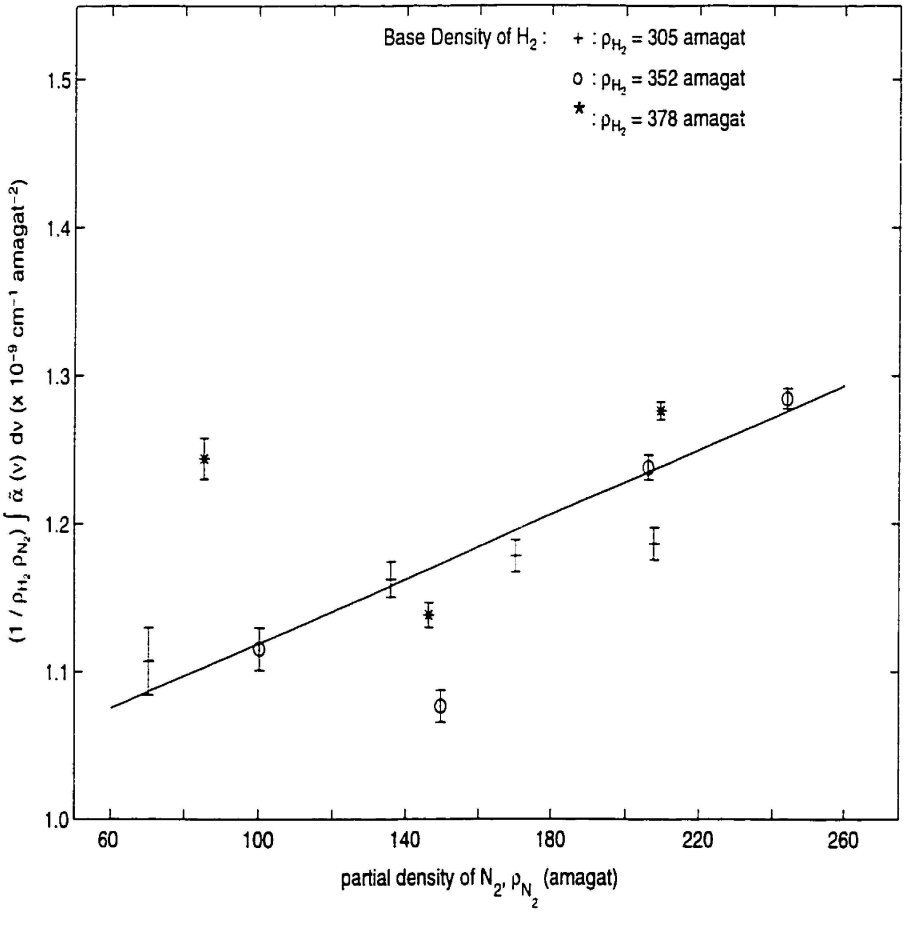


Figure 4.10: A plot of $(1/\rho_{H_2}\rho_{N_2}) \int \tilde{\alpha} d\nu$ versus $\rho_{N_2}$ at 201 K.

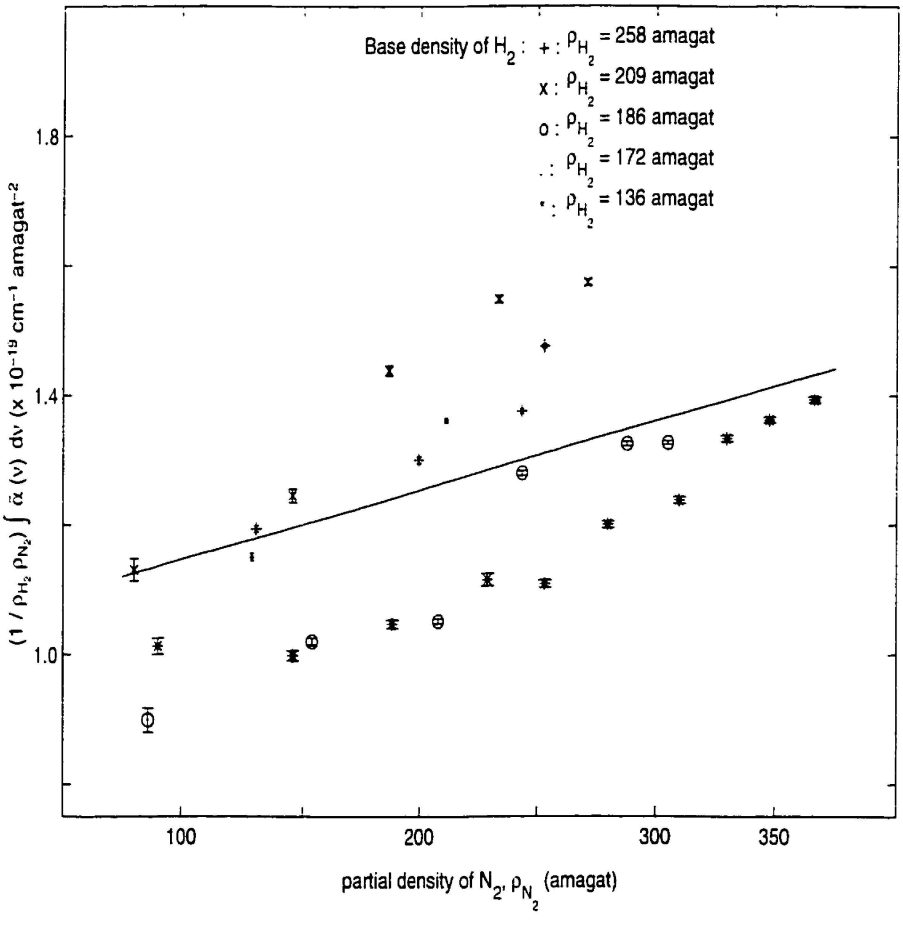


Figure 4.11: A plot of $(1/\rho_{H_2}\rho_{N_2}) \int \tilde{\alpha} d\nu$ versus $\rho_{N_2}$ at 298 K.

# Chapter 5

## Summary

The research project for the present thesis consisted of a systematic experimental study of the collision-induced infrared absorption of the double vibrational transitions $H_2(v = 1 \leftarrow 0) + N_2(v = 1 \leftarrow 0)$ in the spectral region 5600 - 7600 $cm^{-1}$ . The spectra were investigated in a 2 m stainless steel absorption cell for eight different base densities of $H_2$ in the range of 135 to 358 amagat and many partial densities of $N_2$ in the range 70 to 366 amagat, at 201 K and 298 K.

The CIA transitions in the double vibrational spectrum of $H_2$+$N_2$ occur on the high wavenumber wing of the CIA enhancement spectrum of the fundamental band of $H_2$ in $H_2$+$N_2$ mixtures. The observed double vibrational transitions include the following: $O_1(3) + Q_1(J)$ , $O_1(2) + Q_1(J)$ , $Q_1(J) + O_1(J)$ , $Q_1(J) + Q_1(J)$ , $Q_1(J) + S_1(J)$ , $S_1(0) + Q_1(J)$ , $S_1(1) + Q_1(J)$ , $S_1(2) + Q_1(J)$ , and $S_1(3) + Q_1(J)$ , in which the first component is from $H_2$ and the second component is from $N_2$.

A method of profile analysis used in this work is successful in separating the high wavenumber tail of the enhancement of the CIA fundamental band of $H_2$, in $H_2$+$N_2$ mixtures. Lewis-Birnbaum-Cohen (LBC) lineshape function gives the best fit of the calculated profiles to the experimental profiles. The lineshape parameters $\tau_1$, and $\tau_2$ are determined from the analysis for all the experimental profiles. $\tau_1$, and $\tau_2$ are found to be dependent upon the partial density of nitrogen. $\rho_{N_2}$. In particular, the increase of $\tau_1$ with $\rho_{N_2}$ shows a decrease in the line widths (i.e., line narrowing) with increasing $\rho_{N_2}$ at both 201 and 298 K. Finally the binary and ternary absorption coefficients were determined

for the double vibrational transitions of $H_2$+$N_2$ .

# Appendix A

## Methods of analysis and relevant descriptive statistics

During the course of the numerical analysis in the present work, considerable care was taken to obtain the most meaningful estimates of the parameters and the corresponding uncertainties. This was achieved in part by using standard error propagation methods throughout the calculations, as well using defined probability limits (5%) in making all judgements of acceptance, thus eliminating personal bias and strengthening the likelihood of repeatability. In this appendix different techniques used in the numerical analysis are described.

### A.1 Nonlinear Least-Squares Fitting

The two main goals in fitting a model to the experimental data are: to achieve the best fit between the model and the data, and to obtain the most meaningful estimates of the parameters $P_j$ and their confidence limits. To accomplish the first there must be some quantitative measure of the quality of a fit. The most commonly used criterion for this purpose is the $\chi^2$ statistic, defined as

$$\chi^2 = \sum_{i}^{N} \left[ \frac{y_{calc}(i) - y_{obs}(i)}{\sigma(i)} \right]^2 , \tag{A.1}$$

where $\sigma(i)$ is the uncertainty of the observed datum $y_{obs}(i)$, $y_{calc}(i)$ is the corresponding value predicted by the model, and $N$ is the number of the observed data. Thus the best fit would be defined as the one that minimizes equation A.1. This minimization is nontrivial if the equation is nonlinear in the parameters (as is the case here for the

lineshapes used in the present work). This nonlinearity forces the use of an iterative algorithm. Convergence problems to local minimum are a concern, as the actual absolute minimal solution might be very different from the initial choice of parameters. Stability checks are therefore necessary which means choosing many initial parameter sets to insure that the minimal solution is absolute and not local. In addition to the nonlinear problems, there are also some general difficulties with the use of least-squares techniques on real life data. These are discussed in some detail in section A.3.

As for the second goal, it seems intuitively apparent from an intuitive sense that this would be achieved simultaneously with the first. However, such is not the case. Even if a high quality fit is obtained, this does not necessarily indicate a well defined set of parameters. The correlation among the parameters cannot be ignored. Correlation between two parameters $(j, k)$ is defined as

$$C_{jk} = \frac{\sum_i \phi_j(i)\phi_k(i)}{\sqrt{\sum_i \phi_j(i)^2 \sum_i \phi_k(i)^2}}. \tag{A.2}$$

where, $\phi_j(i)$ and $\phi_k(i)$ are the partial derivatives of $y_{calc}(i)$ with respect to the parameters $P_j$ and $P_k$. Equation A.2 defines a number in the range from -1 to 1, and is a measure of how a change in one parameter can be compensated by a change in the other parameter. Correlation causes many problems in nonlinear least-squares (NLLS) based on the simple fact that highly correlated systems can have solution sets with statistically identical $\chi^2$ (differences $\ll 1$) but widely different parameter sets (differences $\gg$ the uncertainties), thus it is very difficult to find the absolute minimum among all the local optimal solutions.

Since NLLS is an iterative process, there is a need for a test for convergence. A common method is to check the change in $\chi^2$ between each iteration and terminate the fit when it falls below some point that is no longer statistically significant. The problem with this is that if a parameter set is strongly correlated it is possible to have an iteration with

a $\chi^2$ change that is negligible, and yet it produces very large changes in the parameters (meaning each parameter change when considered individually would significantly alter the $\chi^2$). This problem was considered in detail by Watson[61], whose basic reasoning was: of central importance is the stabilization of the calculated values $y_{calc}(i)$, thus if the change in a parameter will not make a significant change to these predicted values when considered individually, convergence has been achieved. The problem then is to determine what a significant change in $y_{calc}(i)$ is. If the statistic $\overline{\sigma}_e$ (weighted rms deviation or standard error) is defined as

$$\overline{\sigma}_e^2 = \frac{N}{N-M} \frac{\sum w(i)[y_{calc}(i) - y_{obs}(i)]^2}{\sum w(i)}, \tag{A.3}$$

where $M$ is the number of floated parameters and w(i) is the weight $(=1/\sigma(i)^2)$, the answer becomes clear. Using standard error analysis, an error is considered insignificant if it is at least an order of magnitude less than the dominant error being considered. Now since $\overline{\sigma}_e$ is a measure of the "average" deviations between the numerical model and the actual data, if a change in the parameter set changes $\overline{\sigma}_e$ by less than 10 % the parameter sets are not significantly different, i.e., convergence has been achieved. Therefore the maximum individual parameter change in a set of $M$ parameters, that can be ignored should alter the predicted values $y_{calc}(i)$ by $0.1/M\overline{\sigma}_e$. This is the convergence criterion suggested by Watson. Premature convergence can no longer occur by highly correlated parameters each changing the $\chi^2$ in such a way that the sum of their changes is negligible. With the convergence now determined by the parameter sensitivities, each parameter change has to individually produce no significant change to the predicted values. The parameter sensitivities, $PS_J$, are calculated using standard error propagation methods, and the above criteria, and are given by

$$PS_j = \frac{0.1}{M} \frac{\overline{\sigma}_e}{\phi_j^{rms}}, \tag{A.4}$$

where $\phi_j^{rms}$ is just the root mean square value of $\phi_j(i)$ . When the change in $\chi^2$ is small the ratio of the parameter changes to the parameter sensitivities is a direct indication of how each parameter is correlated to all the other parameters. The larger this ratio is, the more correlated are the parameters.

## A.2 Model Testing

Two common concerns in least-squares fitting are how to test the significance of a fit, and how to test the significance of adding an additional term to a particular model. The $\chi^2$ statistic is often used to test the quality of the fit. The probability that the observed chi-square for a correct model will exceed a given $\chi^2$ is given by

$$Q(\chi^2|\nu) = \gamma_q(\frac{\nu}{2}, \frac{\chi^2}{2}). \tag{A.5}$$

Here $\nu = N - M$ is the number of degrees of freedom, and $\gamma_q$ is the incomplete gamma function defined as

$$\gamma_q(a, x) = \frac{1}{\Gamma(a)} \int_x^\infty e^{-t} t^{a-1} dt, \tag{A.6}$$

where $\Gamma(a)$ is the gamma function given by

$$\Gamma(a) = \int_0^\infty t^{z-1} e^{-t} dt. \tag{A.7}$$

Thus using the standard 5% test of significance, if the probability calculated from equation A.5 is less than 5%, one can assume that either the model chosen is a poor representative of the data, or the uncertainties assigned to the data are a poor representative

of the actual errors. Determining which of these is the case is achieved by examining the calculated and measured results to see if the same general tendencies are present, and comparing the standard error to the rms uncertainty.

To answer the second question, the significance of additional terms is not as trivial as it may seem. Just because the $\chi^2$ decreases this does not indicates a "better" fit. Adding additional parameters will always lower the $\chi^2$. This decrease in $\chi^2$ has to be tested for statistical significance. The $F$ statistic is often used to do this and it defined as follows

$$F_\chi = \frac{\Delta\chi^2}{\chi^2_\nu}. \tag{A.8}$$

Here, $\Delta\chi^2$ is the change in $\chi^2$ when the additional parameter is floated, and $\chi^2_\nu$ is the reduced $\chi^2$ of the model without the additional parameter being floated ($= \chi^2/(N-M)$). This is a probability distribution with degrees of freedom $\nu_1 = 1$ and $\nu_2 = N - M - 1$. The probability that $F$ would be as large purely do to random chance is given by

$$Q(F|\nu_1,\nu_2) = I_{\frac{\nu_2}{\nu_2+\nu_1 F}}(\frac{\nu_2}{2},\frac{\nu_1}{2}). \tag{A.9}$$

Where the $I$ is the incomplete beta function

$$I_x(a,b) = \frac{1}{B(a,b)}\int_0^x t^{a-1}(1-t)^{b-1}dt \tag{A.10}$$

and $B$ is the beta function, given by

$$B(z,w) = \frac{\Gamma(z)\Gamma(w)}{\Gamma(z+w)}. \tag{A.11}$$

Thus again using the standard 5% probability criterion for significance, if the value of $F$ calculated from equation A.9 is less than 5% the additional parameter is meaningful. The above two tests were used throughout the numerical analysis in the present work in the described manner. For example, in determining a suitable order of polynomial to use

in the density vs pressure fits (see section 2.5), the procedure was simply to start from zero order and increase until terms stopped being significant as indicated by testing the $F$ statistic as described above.

## A.3 Robust Weighting

The main problem with least-squares fitting appears when the data have outliers, the results will be greatly skewed. There are more robust methods[62] of fitting that can eliminate this problem, however unlike the regular least-squares methods there is no widely available ready-to-use code. However, it is possible to readily incorporate the central idea of robust methods (give less weight to outliers in the fitting process), into standard least-squares methods[63]. The algorithm is straightforward. First an initial fit using the estimated uncertainties to calculate the weights is done. Then if outliers are present the data is reweighted to compensate for them. This procedure is repeated until convergence is achieved.

To reweight the data to remove the effect of the outliers the following formula is used

$$W(i) = \frac{1}{\sigma(i)^2 + \alpha[y_{calc}(i) - y_{obs}(i)]^2}. \tag{A.12}$$

The test statistic for convergence is written as

$$\sum_i \frac{[y_{calc}(i) - y_{obs}(i)]^2}{W(i)^2} = 1. \tag{A.13}$$

Equation A.13 can also be used to determine the value of alpha (this is a nonlinear equation and is solved similar to equation 2.2) to be used after the first NLLS fit. It may also be necessary to recompute the value of alpha after each step if equation A.13 becomes negative; this means the weights have been over-compensated.

If the notion of outliers to ranges of data rather than individual points is applied, robust weighting can be a very useful tool in CIA analysis. For example how would one fit a spectrum that has some unknown effect perturbing a specific region. One way is to simply not fit that area of the spectrum at all. However this is not an optimal solution for several reasons such as (i) to some extent the absorption must be bounded even in the perturbed regions, and (ii) this manual removal can get tedious since the results of the fit may prompt reassignment of what is perturbed creating a cyclic process. Instead if robust weighting can be used both these problems are avoided. An initial choice of the perturbed regions is made, they are assigned a weight of zero and the above robust algorithm is started. The initial choice is very important, as with different starting weights, different sets of solutions are obtained. This is why the fit must be inspected to insure that the perturbations are bounded correctly. It is important to note that the effect of robust fitting will not reduce the standard error as calculated by equation A.3. What robust fitting does accomplish is the minimization of the median deviation. For data sets with outliers or non-normal distributions median statistics are much more meaningful than mean-based statistics.

## A.4 Parameter Reporting

Even when all the problems associated with least-squared fitting and the model fitted to the data are solved, there are still other decisions to be made. One non-trivial decision is the determination of the number of digits that should be reported when presenting the fitted parameters. From a purely computational point of view, the best method is to retain all digits to the maximum calculating capacity. What would be optimal, however, is a method of minimizing the number of digits quoted without losing significant information, meaning the parameters reported can reproduce the predicted values calculated

from the unrounded parameters.

One common method is to simply round the value according to its uncertainty. As rounding a number introduces a random uncertainty equal to 0.5 times the rounding limit, it is necessary to quote to at least 2 places in the uncertainty and round accordingly. This insures that the roundoff error added to the parameter is an order of magnitude less than its uncertainty. However, this method is not recommended because the uncertainty of a parameter is the amount that it has to be altered to change the $\chi^2$ by $\pm 1$ when the other parameters are floated so as to reminimize the $\chi^2$. In the above case the other parameters are not being reoptimized so the end result could easily be a set of parameters which substantially alters predictions yielded by the model (change the $\chi^2$ by much greater than $\pm 1$). This is clearly not acceptable.

One solution is to round parameters according to their sensitivities[61] as by the definition of the sensitivities this will insure that the effect of rounding all parameters will be an insignificant change in the predicted values (an order of magnitude smaller than the rms error). It is possible, however, to further reduce the number of digits reported without losing meaningful information. Noting that the problem with rounding via the uncertainties was that the other parameters were not allowed to reminimize the fit, the obvious solution is to let them do so[64]. Thus the parameters are rounded off one by one, and the model is refit after each rounding with the rounded parameters being held constant. In general the parameters should be rounded in order of significance from the greatest to the least.

## A.5 Confidence Intervals (Montecarlo Techniques)

When fitting data with a non-normal distribution (large tails) one cannot interpret the covariance matrix from a standard least-squares routine as the actual standard errors

of the parameter estimation. Instead the following must be done[44]; the original data set $S^0$ is fitted to obtain an estimation of the parameters $P^0$; pseudo data sets $S^i$ are constructed by randomly altering the original data set (using an appropriate probability distribution); and each of these data sets is fitted to obtain parameter estimates $P^i$. The differences $P^0 - P^i$ describe the distribution from which confidence intervals for the parameters can be constructed.

The above algorithm was used somewhat in reverse to test the assumption that the experimental errors for the present work were in fact normal. This was achieved by taking the final averaged data set $S^0$ and fitting it to obtain $P^0$, then fitting each of the original data sets to produce the parameters sets $P^i$. The uncertainty estimates from the fit to $S^0$ were then checked to see if they accounted for the scatter $P^0 - P^i$. This was tested for a number of data sets and found to give reasonable indication that the errors were indeed normal, and thus the covariance matrix from the fit to $S^0$ could be used to obtain parameter uncertainty estimates.

## A.6 Basic Statistics

There are the two main descriptive statistics of central tendency of a set of $N$ data, $x_i$, that have uncertainties, $\sigma_i$. The first is the weighted mean, $\mu$, and the second is the error in the weighted mean $\sigma_\mu$ . These are defined as follows

$$\mu = \frac{\sum_i^N w_i x_i}{\sum_i w_i}. \tag{A.14}$$

and

$$\sigma_\mu^2 = \frac{1}{\sum_i^N w_i}. \tag{A.15}$$

In the above equations, the weights $w_i = 1/\sigma_i^2$. As a check, to determine if the weights represent the uncertainties well, $\sigma_\mu^2$ can also be calculated by

$$\sigma_\mu^2 = \frac{\sum_i^N w_i(x_i - \mu)^2}{\sum_i^N w_i} \frac{N}{N-1}. \tag{A.16}$$

These two equations should be approximately the same, the advantage of equation A.16 is that the weights only need to be relative.

## A.7 Error Analysis

There are two basic methods of calculating the uncertainty in the value of a function, $f$, when its set of $i$ variables, $a_i$, have uncertainty, $da_i$ . The first and most common method is to use differential calculus and the uncertainty is defined as

$$df(a)^2 = \sum_i \left[ \left( \frac{\delta f}{\delta a_i} \right)_a da_i \right]^2. \tag{A.17}$$

The second method is to use the actual definition of uncertainty which defines is as the the amount that the function will change when its variables are changed by its uncertainty. This is represented by

$$df^2 = \sum_i [f(a + da_i) - f(a)]^2. \tag{A.18}$$

The advantage of equation A.17 is that it is often much faster to compute if analytic expressions for the partial derivatives are available. Sometimes though its simpler to use equation A.18, for example, when dealing with the nonlinear equations in section 2.6.

## Appendix B

### On Astrophysical Applications of CIA Spectra

In this Appendix we give a brief outline of the astrophysical applications of collision-induced absorption spectra of nonpolar molecules.

Herzberg[65] identified a weak absorption feature at 0.8270 $\mu m$, observed by Kupier[66] in Uranus and Neptune, as the $S_3(0)$ transition of $H_2$ in the second overtone band of its CIA spectrum. As a matter of fact this observation constitutes the first detection of molecular hydrogen in a planetary atmosphere. A broad weak feature at 0.6420 $\mu m$ in the spectra of the same two planets was observed by Spinrad[67] as the $S_4(0)$ component of the third overtone band of $H_2$. Trafton[68] discussed the CIA spectra of $H_2$ including its pure translational and rotational-translational spectra[3] in the far infrared which are important from the point of view of energy bands in the planets of the solar system.

The CIA of the fundamental band of $H_2$ at 2.4 $\mu m$ was observed as a broad feature in the spectrum of Jupiter by Danielson[69]. Welsh[70] discussed the applications of CIA spectrum of the $H_2$ to the study of planetary atmospheres.

Belton and Spinrad[71] suggested from their observation (photoelectrically) of the ratio of the CIA spectra of the $S_3(0)$ line in the 3-0 band of $H_2$ of Uranus and Neptune that there is similarity of the two atmospheres. Danielson[72] proposed that the absorption features in the spectrum of Uranus around 0.6000 $\mu m$ primarily arises from simultaneous double transitions of $H_2 + CH_4$ and that these transitions may also provide the continuum absorption between the pure $CH_4$ bands.

The Earth and Titan (one of the moons of Saturn) are two solar system bodies whose

atmospheres are composed predominantly of $N_2$[73, 74, 75]. The phenomenon of collision-induced absorption arising from collisions of $H_2$+$N_2$ plays a role in the atmosphere of Titan as discussed by Hunt et. al.[76] .

The present Appendix outlines briefly the applications of the CIA spectra of some major planets as well as those of Earth and Titan. The reader is referred to the references given in this note, as well as additional references given there, for exhaustive description of the application of the CIA spectra of $H_2$ and $N_2$ in their pure state and in the binary mixtures such as $H_2$ + $N_2$ .

## Bibliography


[1] M. F. Crawford , H. L. Welsh and J. L. Locke . *Phys. Rev.*, 75:1607, 1949.

[2] H. L. Welsh, M. F. Crawford, and J. L. Locke. *Phys. Rev.*, 76:580, 1949.

[3] H. L. Welsh. *in MTP International Review of Science, Physical Chemistry, Vol. 3. Spectroscopy.* edited by D. Ramsay (Butterworths, London, 1972).

[4] S. P. Reddy. *in Phenomena Induced by Intermolecular Interactions.* edited by G. Birnbaum (Plenum, New York, 1985).

[5] C. W. Hsieh. *Ph. D. Thesis, Memorial University of Newfoundland.* 1992.

[6] N. H. Rich and A. R. W. McKellar. *Can. J. Phys.*, 54:486, 1976.

[7] J. L. Hunt and J. D. Poll. *Mol. Phys.* 59:163, 1986.

[8] J. Van Kranendonk. *Physica.*, 73:156, 1974.

[9] J. D. Poll. *Proceedings of the International School of Physics Enrico Fermi, Course LXXV. Intermolecular Spectroscopy and Dynamical Properties of Dense Systems.* North-Holland Publishing Company, New York, 1980.

[10] G. Birnbaum, B. Guillot, and S. Bratos. *Adv. Chem. Phys.*, 51:49, 1982.

[11] L. Frommhold. *Collision Induced Absorption in Gases.* (Cambridge University Press, Cambridge, 1993).

[12] J. Van Kranendonk. *Physica.*, 23:825, 1957.

[13] J. D. Poll and J. Van Kranendonk. *Can. J. Phys.*, 39:189, 1961.

[14] J. D. Poll and J. L. Hunt. *Can. J. Phys.*, 54:461, 1976.

[15] J. Van Kranendonk. *Can. J. Phys.*, 46:1173, 1968.

[16] J. C. Lewis, and J. Van Kranendonk. *Phys. Rev. Lett*, 24:802, 1971.

[17] J. C. Lewis, and J. Van Kranendonk. *Can. J. Phys.*, 50:325, 1972.

[18] J. C. Lewis, and J. Van Kranendonk. *Can. J. Phys.*, 50:2902, 1972.

[19] J. C. Lewis. *Can. J. Phys.*, 50:352, 1972.

[20] J. C. Lewis. *Can. J. Phys.*, 50:2881, 1972.

[21] J. C. Lewis. *Can. J. Phys.*, 51:2455, 1973.

[22] J. C. Lewis. *Physic A.*, 82A:500, 1976.

[23] J. C. Lewis. *Phenomena Induced by Intermolecular Interactions, edited by G. Birnbaum (Plenum Publishing Corporation, New York)*, page 215, 1985.

[24] A. R. W. McKellar and H. L. Welsh. *Proc. Roy. Soc. London A*, 322:421, 1971.

[25] S. P. Reddy, G. Varghese, and R. D. G. Prasad. *Phys. Rev.*, A 15:975, 1977.

[26] E. van Nostrand. *M.Sc. Thesis, Memorial University of Newfoundland*, 1983.

[27] G. Varghese, R. D. G. Prasad, and S. P. Reddy. *Phys. Rev.*, A 35:701, 1987.

[28] A. R. W. McKellar. *Can. J. Phys.*, 66:155, 1988.

[29] J. De Remigis, J. W. Mactaggart, and H. L. Welsh. *Can. J. Phys.*, 49:381, 1971.

[30] J. W. Mactaggart, J. De Remigis, and H. L. Welsh. *Can. J. Phys.*, 51:1971, 1973.

[31] S. P. Reddy and C. W. Cho. *Can. J. Phys.*, 43:2331, 1965.

[32] M. M. Shapiro,and H. P. Gush. *Can. J. Phys.*, 44:949–963, 1966.

[33] W. J. Lafferty, A. M. Solodov, A. Weber,W. M. Olson, and J. M. Hartman. *Applied Optics*, 35:5911–5917, 1996.

[34] S. L. Bragg, J. W. Brault, and W. H. Smith. *Astrophys. J.*, 263:999, 1982.

[35] A Lofthus,and P. Krupenie. *J. Phy. Chem. Ref. Data*, 6:113–307, 1977.

[36] K. Huber, and G. Herzberg. *Molecular Spectra and Molecular Structure IV. Constants of Diatomic Moleculas.* Van Nonstrand Reinhold, New York, 1979.

[37] B. Vodar. *Spectro. Chemic. Acde.*, 14:213–233, 1959.

[38] J. C. Lewis. *private communication.*

[39] G. Birnbaum and E. R. Cohen. *Can. J. Phys.*, **54**:593, 1976.

[40] C. W. Hsieh. PhD thesis, Memorial University of Newfoundland, 1992.

[41] P. G. Gillard. PhD thesis, Memorial University of Newfoundland, 1983.

[42] R. D. McCarty,J. Hord, and H. M. Roder. *Selected Properties of Hydrogen.* NBS, Wasgington, DC, 1981.

[43] A. Michels , R. J. Lunbeck, and G. J. Wolkers. *Physica.*, 17:9:801–816, 1951.

[44] Philip R. Bevington and D. Keith Robinson. *Error analysis for the physical sciences.* McGraw-Hill, Inc., New York, 1992.

[45] P. L. Jolivette. *Computers in Physics*, 7:2:208:212, 1993.

[46] A. N. Zaidel, V. K. Prokofer, S. M. Raisku, V. A. Slavnyl, and E. Ya. Shreider. *Tables of Spectral Lines*. IFI/Plenum, New York-London, 1970.

[47] A. R. Downie,M. C. Magoon, Thomasine Purcell, and Bryce Crawford, Jr. . *Journal of the Optical Society of America*, 43:11, 1953.

[48] J. D. Poll. *Proceedings I.A.U. Symposium 40 on Planetary Atmospheres (Reidel, Dordrecht)*, page 384, 1971.

[49] G. Karl,J. D. Poll, and L. Wolniewicz. *Can. J. Phys.*, 19:1781, 1975.

[50] M. E. Rose. *Elementary Theory of Angular Momentum*. John Wiley & Sons, Inc., New York, 1957.

[51] J. L. Hunt, J. D. Poll, and L. Wolniewicz. *Can. J. Phys*, 62:1719, 1984.

[52] P. G. Gillard. *paper on D2 at 77 K*, 1984.

[53] S. P. Reddy, A. Sen, and R. D. G. Prasad. *J. Chem. Phys.*, 72:6102, 1980.

[54] J. C. Lewis, and J. A. Tjon. *Physica A*, 91:161, 1978.

[55] P. A. Egelstaff. *Proceedings Symposium on Inelastic Neutron Scattering, IAEA*. Vienna, 1960.

[56] A. Borysow, and L. Frommhold. *Astrophys. J.*, 311:1043, 1986.

[57] A. Borysow, L. Frommhold, and W. Meyer. *Physica A*, 40:6931–6949, 1989.

[58] W. Meyer, A. Borysow, and L. Frommhold. *Physica A*, 47:4065–4077, 1993.

[59] A. Borysow, L. Frommhold, and W. Meyer. *Physica A*, 41:264–270, 1990.

[60] J. Boissoles, R. H. Tipping, and C. Boulet. *J. Quant. Spectrosc. Radiat. Transfer*, 51:615–627, 1994.

[61] J. K. G. Watson. *J. Mol. Spect.*, 66:500–502, 1977.

[62] A. F. Ruckstuhl,W. A. Stahel,and K. Dressler. *J. Mol. Spect.*, 160:434–435, 1993.

[63] J. K. G. Watson. *private communication*, 1994.

[64] R. Le Roy. Paper FB10. 52nd Ohio State University International Symposiumm on Molecular Spectroscopy, 1997.

[65] G. Hertzberg. *Astrophys J.*, 115:337–340, 1952.

[66] G. P. Kupier. *Astrophys. J.*, 109:540–541, 1949.

[67] H. Spinrad. *Astrophys. J.*, 138:1242–1245, 1963.

[68] L. M. Trafton. *Astrophys. J.*, 140:1340, 1964.

[69] R. E. Danielson. *Astrophys. J.*, 143:949–960, 1966.

[70] H. L. Welsh. *J. Atmos. Sci.*, 26:835, 1969.

[71] M. J. S. Belton,and H. Spinrad. *Astrophys. J.*, 185:363–372, 1973.

[72] R. E. Danielson. *Astrophys. J.*, 192:L107–L110, 1974.

[73] R. E. Samuelson, R. A. Hanel, V. G. Kunde, and W. C. Maguire. *Nature*, 292:688–693, 1981.

[74] W. C. Maguire, R. A. Hanel, D. E. Jennings, V. G. Kunde, and R. E. Samuelson. *Nature*, 292:683–686, 1981.

[75] V. G. Kunde.A. C. Aiken,R. A. Hanel.D. E. Jennings,W. C. Maguire.and R. E. Samuelson. *Nature*. 292:686–688, 1981.

[76] J. L. Hunt. *Icarus*. 55:63–72, 1983.